The Pennsylvania State University

The College of Health and Human Development

Department of Kinesiology

SOFT TISSUE OSCILLATION INCREASES GAIT STABILITY IN PASSIVE-DYNAMIC WALKERS

A Thesis in

Kinesiology

by

Samuel E Masters

Submitted in Partial Fulfillment
of the Requirements
for the Degree of

Master of Science

May 2015

The thesis of Samuel Edward Masters was reviewed and approved* by the following:

John H Challis
Professor of Kinesiology
Thesis Advisor

Robert B Eckhardt
Professor of Developmental Genetics and Evolutionary Morphology

Stephen J Piazza
Professor of Kinesiology
Program Director, Graduate Program

*Signatures are on file in the Graduate School

ABSTRACT

The majority of human body mass is comprised of soft tissue which can oscillate during human locomotion. Models of human locomotion that contain a soft-tissue component can be used to study the potential role of soft-tissue oscillations. Passive-dynamic walkers (PDWs) are models of human ambulation that can be used to study the underlying dynamics of walking gait. Passive-dynamic walkers can ambulate on an incline solely due to gravity. A PDW with a soft-tissue component was modeled to study the effects of soft-tissue oscillation on human gait dynamics. The control passive-dynamic walker (CPDW) contained point masses at the hip and at each foot. The legs were massless and rigid. The oscillating passive-dynamic walker (OPDW) was identical to the CPDW except for the addition of spring-mass-damper system attached to the hip mass to simulate soft-tissue oscillation. Floquet multipliers (FMs), local divergence exponents (LDEs), the basin of attraction (BOA), slope perturbation range (SPR), and step time variability (STV) were utilized to access stability. Floquet multipliers and LDEs measure short-term step-to-step and short-term inter-step stability, respectively. The BOA measures long-term step-to-step stability. Slope perturbation range and STV measure PDW robustness to uneven terrain in the short-term and long-term, respectively. The spring-damper parameters of the OPDW could be tuned such that the gait stability of the OPDW was greater than that of the CPDW by 38.1%, 6.2%, 135.1%, 131.9%, and 40.3% for the FMs, LDEs, the BOA, the SPR, and the STV, respectively. The walking gait of the PDW model with a soft-tissue component was more stable than the fully rigid

model. This suggests damped soft-tissue oscillations may, in addition to their other roles, make human gait more stable.

TABLE OF CONTENTS

LIST OF FIGURES

LIST OF TABLES

ACKNOWLEDGEMENTS

I have had a wonderful experience collecting and analyzing data with the help of my advisor, Dr. John H. Challis, and lab partner, Justin C. Wager. Thank you for the guidance and the many conversations that helped mold my interests in the realm of biomechanics. I would also like to thank my committee members Dr. Stephen J. Piazza and Dr. Robert B. Eckhardt. And, finally, I would like to thank my future wife, Ms. Loren Archibeque, who brings love and stability to my life of *chaos*.

Chapter 1

Introduction

1.1 General Introduction

Animal locomotion is one of the most deeply studied areas of biomechanics. Giovanni Borelli gave extensive thought on the movement of animals in the 1600's. Fast forward about 200 years and you could meet Edward Muybridge who took photographs of horses galloping to deduce whether their trotting gait contained a flight phase. Muybridge also took photographs of humans *au naturel* in order to characterize and study human walking. Humans are great subjects for the study of bipedal locomotion. Humans are versatile and come in many shapes and sizes. However, depending on the research questions, this may be the biggest drawback of human subjects. Humans are made up of many musculoskeletal and mechanical degrees of freedom. The coordination of the neuromuscular system with the inertial dynamics of the human body is complex and near impossible to perfectly simulate. Instead, simpler models are constructed in order to piece out the components of the human body and their contributions to movement.

Passive-dynamic walkers typically consist of a series of point mass or rigid bodies that are linked via hinge joints. Given the right initial conditions these bipedal walkers can achieve stable walking cycles down an incline with gravity as the only power source. Due to the absence of a control system, they serve as a great tool to study the primal

dynamics of bipedal walking. Furthermore, they can be modified to study different components of the human body and their effects on gait dynamics.

1.2 Purpose of Study

The human body is primarily made up of mass that can oscillate during locomotion. The vast majority of models for the human body consist of masses that are completely rigid. However, tissue that oscillates during locomotion would have a dynamical consequence on the stability of bipedal gait. A purpose of the study was to quantify and assess the dynamic stability of a passive-dynamic walker with a soft tissue component compared to a passive-dynamic walker without a soft tissue component. Furthermore, another purpose of the study was to quantify the effects of soft tissue parameter variation on the dynamic stability of a passive-dynamic walker.

1.3 Specific Aims

The specific aims of the study were the following:

1. To study the effects of soft tissue with varying spring-damper parameters on the orbital stability of passive-dynamic walking by calculating the maximum Floquet multiplier of period-1 stable gait cycles.
2. To study the effects of soft tissue with varying spring-damper parameters on the local stability of passive-dynamic walking by calculating the principal local divergence exponent of period-1 stable gait cycles.

3. To study the effects of soft tissue with varying spring-damper parameters on the global stability of passive-dynamic walking by calculating the basin of attraction for the fixed point of period-1 stable gait cycles.
4. To study the robustness of a passive-dynamic walker with and without a soft-tissue component on rough terrain.

1.4 Study Overview

In this study a passive-dynamic walker with soft tissue was simulated in order to examine the effects of soft tissue on gait stability. Many different aspects of stability were measured: orbital stability, local stability, global stability, and general robustness to external perturbations and perturbations in the environment. The spring-damper parameters were systematically varied and the changes to gait stability were examined. The passive-dynamic walker with a soft tissue component was compared to a passive-dynamic walker without a soft tissue component.

1.5 Thesis Structure

Chapter two of this thesis contains a literature review that focuses on passive-dynamic walkers, human walking, and human soft tissue properties. Chapter three is an overview of the methods that were utilized to examine the role of soft tissue on the stability of bipedal walking. Chapter four reveals the results of the dynamic analysis on gait and stability. Chapter five discusses the implications of the results on passive-

dynamic walking and human walking. An appendix and the references follow chapter five.

Chapter 2

Literature Review

2.1 Introduction

Human locomotion manifests in many different forms. Each form is primarily dictated by the goal (e.g., running to maximize speed, walking to minimize energy expenditure, or crawling to complete a unique task). The most common form of human locomotion is walking. Walking requires little conscious effort but involves many components of the human body acting simultaneously. It is difficult to determine the specific role that each component (e.g., tendons, muscles, nervous system) of the human body plays during human locomotion. To add another layer of complexity, the functions of each component of the human body are heavily dependent upon each other.

A solution to determine the role of a component within the human body during locomotion is to create a model. Models can greatly reduce the degrees of freedom in order to tease out the role of a single component. Passive-dynamic models are not influenced by neuromuscular dynamics. Rather, they are purely driven by energy supplied from gravity or a simple actuator and the mechanical dynamics. These mechanisms can be easily modified to include (or exclude) simple, representative components of the human body. The following is a summary of literature related to passive-dynamic mechanisms, human walking, and measuring walking stability.

2.2 Passive-Dynamic Walkers

2.2.1 History of Passive-Dynamic Walkers

In 1887, George T. Fallis filed a patent application for a bipedal walking toy. This toy, when placed on a slight incline, could walk with gravity as the only power source. It leaned on one leg to provide a clearance which allowed the opposite leg to swing. Fallis' description of the toy he invented illustrated a simple passive-dynamic walker (PDW). Most passive-dynamic walkers, such as Fallis' toy, exhibit compass gait. Compass gait is such that the pelvis follows the path of an inverted pendulum during each step cycle (McMahon, 1984). The design of the inverted pendulum varies from a simple hinge joint with a point mass located at the proximal end (Garcia et al., 1998) to a rigid body pendulum with a rolling constraint (McGeer, 1990).

McGeer and Palmer (1989) derived the equations of a domino oscillating like an inverted pendulum. However the support of the pendulum transferred from one edge of the domino to the other as the domino oscillated fore and aft (Figure 2-1). The incline of the ground was not assumed to be zero. The transfer of support from one edge to the other was modeled as instantaneous and impulsive to simplify the equations of motion. Furthermore, the domino was assumed to oscillate at small angles such that $\sin(\theta) \approx \theta$.

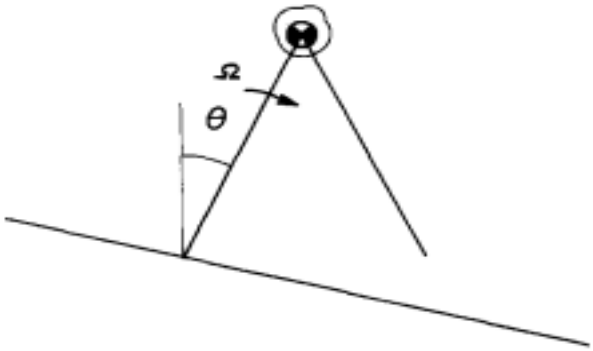

Figure 2-1. A schematic of an oscillating domino that transfers support from one leg to the other. The system has a single point mass connected to both legs. The stance leg angle, θ, is relative to the vertical axis and has an angular velocity of Ω. The stance leg angle is the only degree of freedom for this system (McGeer and Palmer, 1989).

The equations of motion for the inverted pendulum were used to predict the period of one oscillation for an empty VHS box and an aluminum block. A microphone was utilized to measure the sound at each support transfer (Figure 2-2). The microphone provided a means to measure the period of each oscillation and the coefficient of restitution during support transfer. The coefficient of restitution is the ratio of the angular velocity after support transfer to the angular velocity before support transfer. McGeer and Palmer (1989) predicted the coefficient of restitution for the aluminum block and empty VHS tape by assuming that the angular momentum is conserved during the support transfer. The predicted values for the coefficient of restitution were 0.003 greater and 0.008 less than the measured values for the aluminum block and VHS box, respectively. This difference is due to the fact that the transfer of support is not a purely inelastic event.

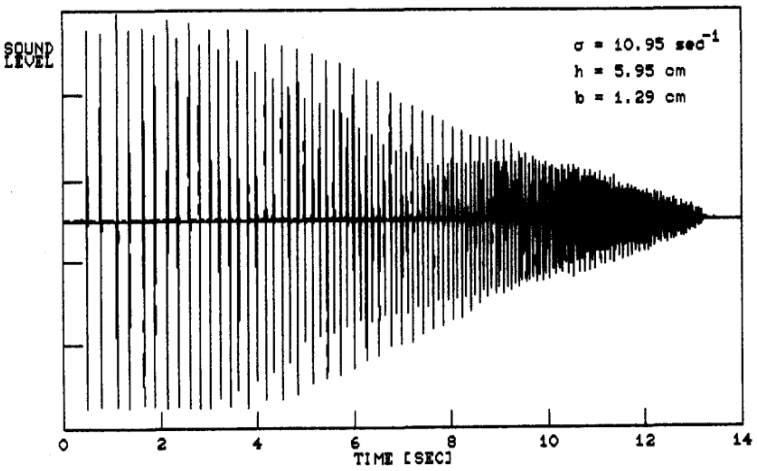

Figure 2-2. A plot of the sound level recorded by a microphone of an aluminum block oscillating fore and aft. The height of the aluminum block, h, was 5.95 cm. The base width of the aluminum block was 1.29 cm. The ratio of the pendulum-mode frequency of the aluminum block to the frequency of a simple pendulum, σ, was utilized to scale time (McGeer and Palmer, 1989).

McGeer (1990) formulated the equations of motion for a bipedal PDW that was partially based on the principles outlined by McGeer and Palmer (1989). McGeer (1990) provided a detailed analysis of the dynamics of said PDW and the effects of parameter variation (e.g., leg length and mass distribution). Furthermore, a physical PDW was

constructed to illustrate that a purely passively mechanism based on the dynamics of an inverted pendulum could achieve stable locomotion. The majority of PDW research has stemmed from the analyses outlined by McGeer (1990). The stability and efficiency of PDWs has been researched extensively. Some PDWs have been modified to study the role of the upper body (e.g., Wisse et al., 2004), assess gait asymmetry (e.g., Gregg et al., 2012), or examine the effects of elastic energy storage and release (e.g., Dean and Kuo, 2009; Hu and Zhao, 2012). Typically these bipedal models are used to examine the different components of the human body that shape walking gait. They serve as a relatively simple model to understand the primal dynamics that dictate the stability and energetic cost of human locomotion.

2.2.2 Model Types

Passive-dynamic walkers have been modeled in many different ways. Passive-dynamic walkers can be very simple (e.g., a rimless wheel) or mildly complex (e.g., rigid body walker with an upper torso supported by torsional springs). Typically, modifications are made to serve a functional purpose (e.g., the addition of a knee joint to eliminate scuffing of the swing foot during mid-swing) or to simulate a biological mechanism of the human body (e.g., soft tissue vibration). The following section will outline some of the more common types of PDWs and passive components that they contain.

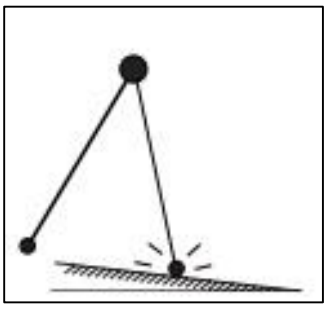

Figure 2-3. A Simple passive walker with four degrees of freedom. The feet and hip were modeled as point masses. The legs are rigid and massless (Garcia et al., 1998).

Garcia et al. (1998) studied one of the simplest and most common PDWs, the *compass walker*. It consisted of a point mass located at the hip and each foot (Figure 2-3). The legs between the feet and hip were rigid and massless. The joint connecting the proximal end of the leg and hip allowed one rotational degree of freedom. The stance foot was connected to the ground via a revolute joint that allowed one rotational degree of freedom.

Garcia et al. (1998) demonstrated this PDW could achieve stable locomotion. A numerical simulation that consisted of a system of first-order differential equations was used to examine the gait cycles on slopes, β, for $0 < \beta < 0.0192$ radians. The phase space of the walker was mapped and the eigenvalues of the Jacobian of said phase space were determined to analyze stability. The PDW exhibited stable locomotion for $\beta < 0.0151$ radians. These gait cycles were period-1 limit cycles. That is, each step was kinematically identical to following step. As the slope increased to 0.0192 radians the gait cycle became unstable and failed to ambulate. The walking velocity increased as the slope increased and the PDW fell forward once the ambulatory velocity was too great for the swing leg to keep up.

Figure 2-4. Kneed PDW with arms. The arms swung in unison with the contralateral thigh (Collins et al., 2001).

Collins et al. (2001) designed a physical, kneed PDW that stood 85 cm tall and weighed 4.8 kg (Figure 2-4). Some of the more common modification to the compass walker

are knees and arms. Knees provide clearance between the foot and ground during leg swing. In an attempt to make the PDW more stable in the frontal plane, Collins et al. (2001) also added arms to the model. Opposite to human arm swing, as the arms of the PDW moved anteriorly they simultaneously swung laterally. The opposite configuration caused the walker to topple, thus illustrating that lateral arm swing affects walking performance. For each trial, the passive walker was placed at the top of a 5-meter ramp and released with added kinetic energy from the handler. If the walker made it down the entire length of the ramp without falling, the trial was deemed successful. The slope that resulted in the most successful trials was 3.1^{o}. The step length was approximately 30 cm, the step period was approximately 0.6 seconds, and the walking speed was approximately 0.51 m/s.

It is common to modify the compass walker by adding a mass that represents the torso or a spring connected to the stance leg and/or swing leg. Wisse et al. (2004) simulated a compass walker with a torso-point mass connected to the hip mass via a rigid and massless bar. Furthermore, to control the step frequency and produce stable walking cycles, a linear spring that connected the stance leg and swing leg was added. Wisse et al. (2004) tested the stability by perturbing the initial conditions of a period-1 gait cycle and determining its *basin of attraction*. The basin of attraction is the set of all initial conditions that resulted in walking that converged to the period-1 gait cycle. The basin of attraction for a period-1 gait cycle was larger than that of the compass walker without a torso and spring component. The stability of the walker was also dependent upon the spring stiffness values. The spring stiffness could be tuned such that the gait cycle was

asymmetric. This behavior is not uncommon in PDWs. Garcia et al. (1998) found that slopes above 0.0151 radians resulted in asymmetric walking.

The behavior of a PDW is highly sensitive to the internal structure of the biped. Therefore the modifications are made with careful consideration of their effects on bipedal gait. Stable walking cycles become increasingly difficult to find as the number of degrees of freedom increase. A common approach to reduce the number of degrees of freedom is to kinematically couple the generalized coordinates. If the number of degrees of freedom is low enough, then analytical solutions of stable gait cycles can be approximated (McGeer, 1990).

2.2.3 Model Applications

Passive-dynamic walkers have a broad range of applications in the study of human walking. An alteration to a PDW may change the gait in a substantial manner. These alterations can represent passive human components and give researchers insights into features of the human body that shape gait.

Passive-dynamic walkers have been modified and utilized as tools to study the role of the nervous system in walking gait. Gates et al. (2007) slightly altered the PDW described by Garcia et al. (1998) by adding a force that propels the swing leg forward on a level slope. The equation for the propulsive force was the sum of theoretical "motor" noise, "sensory" noise, and the required propulsive force that resulted in sustainable walking. Motor and sensory noise had an equal effect on the variability in stride period. The model reproduced variability in the stride period that was similar in magnitude to

published data of healthy and diseased people (Gates and Dingwell, 2007). This PDW is a precursor to understanding the role that higher neurological disorders have on walking gait.

Passive-dynamic walkers are intrinsically efficient due to their ability to walk without actuators, thus they serve as a springboard to designing robots that minimize energy usage. Collins et al. (2005) designed a robot (Cornell robot) based on the PDW presented in Collins et al. (2001). The only power input was from a motor at the ankle that drove push-off. The total power added to this system was nearly equal to the work done on the passive walker driven purely by gravity. The Massachusetts Institute of Technology designed a bipedal robot with ankle actuators and passive hips (Collins et al., 2005). Conversely, the University of Delft designed a bipedal robot with hip actuators and passive ankles (Collins et al., 2005). All three of these bipedal robots walked with a cost of transport similar to that of humans, whereas the Honda Asimo, which is not based on passive walkers, has a cost of transport well above that of a human (Collins et al., 2005). Furthermore, the Cornell and Delft robots were controlled simply by ground contact, which signaled the actuators to turn on or off. This binary feedback control produced gait similar to human walking, whereas the Honda Asimo depended on complex algorithms to determine walking gait from sensory feedback.

2.2.4 Optimization of Models

The compass walker is inherently unstable due to the lack of a feedback controller. However, it is for this reason that the compass walker is an excellent model

for studying how the human body passively or actively stabilizes human locomotion. Biologically inspired components can be added to the system and the parameters of said components can be optimized to maximize the stability of the compass walker. Due to the inherent instability of the compass walker, even small changes in the dynamics of the walker can greatly increase the stability and provide insight into the human body.

Hu and Zhao (2012) optimized the spring stiffness of two PDWs and compared it to a PDW without a spring (PASSIVE). One PDW had a torsional spring acting at the hip (HIP), and the other walker had a linear spring connected to the swing leg's center of mass and the center of mass of both legs (COM) (Figure 2-5). Hu and Zhao (2012) quantified the walking velocity, *v*, and step length, *σ*, of all three models for varying slopes. Hu and Zhao (2012) also quantified the walking trajectory after small state perturbations to measure the walker's gait sensitivity norm (GSN). The GSN, *s*, is a method for measuring when a walker will fall by monitoring gait indicators (e.g., step width, step time, foot-ground clearance) and comparing them to gait indicator values for which the walker is likely to fall (Hobbelen and Wisse, 2007). The walking performance was calculated as,

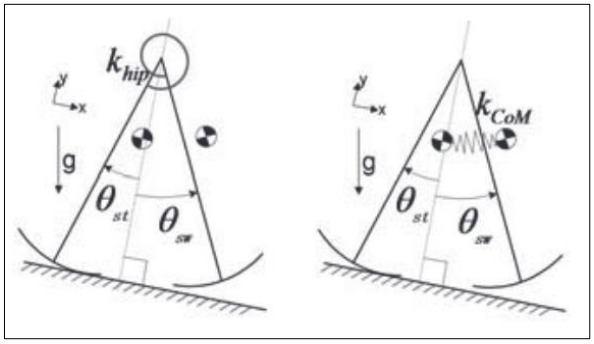

Figure 2-5. The HIP PDW (left) included a torsional spring at the hip. The COM PDW (right) included a linear spring attached at one end to the swing leg's center of mass and to the other end at the center of mass of both legs (Hu and Zhao, 2010).

$$Performance = v.s^3.e^{-\frac{|\sigma-\sigma_0|}{\sigma_0}}$$

where σ_0 is a desired step length of 45% leg length. Hu and Zhao (2012) optimized the spring stiffness and found that the step length decreased, GSN decreased, and walking velocity increased for the HIP and COM models. The COM model had the largest decrease in GSN. Energy expenditure was quantified as a ratio of gravitational potential energy and the product of weight and distance traveled. The HIP and COM models exhibited greater energetic efficiency than the PASSIVE model. Hu and Zhao (2012) illustrated that optimization of spring stiffness may increase gait stability and walking performance in PDWs.

Hass et al. (2006) analyzed the optimal distribution of mass during walking performance of a PDW over varying slopes. The authors maximized walking speed and stability for slopes between 0.0001^o and 15^o by optimizing the mass distribution. Hass et al. (2006) found that the period of one step approached zero as the position of the mass of the swing leg approached the hip and the radius of gyration approached zero. Simultaneously, the basin of attraction decreased which is indicative of a decrease in stability. Hass et al. (2006) also found that as the mass distribution of the stance leg was moved posteriorly, the basin of attraction increased and velocity decreased. As the slope increased the stability decreased and walking velocity increased, therefore the stance leg mass moved posteriorly to compensate for the loss in stability. As the basin of attraction was increased with decreasing slope, the mass could move anteriorly to increase walking velocity. Hass et al. (2006) demonstrated that mass distribution affected the stability and walking velocity of a PDW.

Schuitema et al. (2005) simulated a PDW with a minimal feedback controller located at the hip to stabilize the walker during perturbations in the walking environment.

The authors performed three optimization routines: minimizing cost of transport (CoT), maximizing walking speed, and both simultaneously. Cost of transport was defined as the ratio of external energy added to the system to the product of unit weight and distance traveled. The simultaneous optimization yielded the best results. The average speed was 0.566 m/s and CoT was 0.121 J/m when optimized for both conditions. Furthermore, to test the robustness of the walker, the floor height was randomly varied between steps. The model adapted to changes in floor heights of up to 1.0 cm without failing. Schuitema et al. (2005) demonstrated the ability of a minimal feedback controller to optimize for multiple variables while maintaining robustness.

Researchers have demonstrated that models parameters of a PDW can be tuned and their performance optimized. The human body has many passive components that may influence walking gait, i.e., tendons, ligaments, and other soft tissues. The effect of passive components on walking gait is not fully understood and may be further investigated using PDWs that include these components.

2.3 Human Walking

2.3.1 Features of Walking

Zatsiorky et al. (1994) published a comprehensive review of walking kinematics. One stride is characterized by a right swing/left support phase, a brief double support phase, a right support/left swing phase, then another brief double support phase. Walking velocity (V) is the product of step length (L) and step frequency (F). Step frequency is the most common measurement during walking analysis, and L is typically measured by the quotient of V and F (Zatsiorsky et al., 1994). Yamasaki et al. (1984) measured the L and F for a range of walking speeds and treadmill inclines. Yamasaki et al. (1984) reported two relations: $L = 5.72 \times V^{0.57}$ and $F = 0.294 \times V^{0.43}$. Milner and Quanbury (1970) found a parabolic relation between F and V as well. The critical frequency is the F at which double support phase disappears. That is, it is the F at which walking transitions into running. Critical frequency ranges from 175-200 steps/min in a normal population (Ivanitsky, 1965).

Cavagna et al. (1976) estimated the work done by ten male subjects while walking across a force platform. The vertical ground reaction force (GRF), horizontal GRF, and an estimation of the whole-body center of mass were recorded. The mechanical energy conservation during walking was measured for subject-selected walking speeds. Cavagna et al. (1976) found that at intermediate speeds (approximately 4 km/hr), the

mechanical energy conservation was approximately 65%. The work against gravity increased as the speed decreased below 4 km/hr, resulting in a decrease in mechanical energy conservation. The propulsive work increased as the speed increased above 4 km/hr, resulting in a decrease in mechanical energy conservation. Cavagna et al. (1976) found that the most efficient walking pattern was such that the gravitational potential energy and kinetic energy were out of phase, which is similar to that of an inverted pendulum.

Usherwood et al. (2012) described some defining characteristics of the vertical ground reaction force (GRF) during stance phase of human walking (Figure 2-6). The stance phase in most humans is characterized by heel-sole-toe contact with the ground. During heel contact of the stance phase (I), the total mechanical energy of the center of mass decreases due to energy dissipation. The parabolic displacement of the center of mass occurs primarily during the sole contact, or vault phase (II), of single-leg stance. The vertical GRF during walking is lowest during the vault phase. This phase is characterized by low metabolic cost due to the ground reaction force passing through the ankle, thus reducing the necessity of muscle force production to maintain stability at the ankle (Cavagna et al., 1977). During

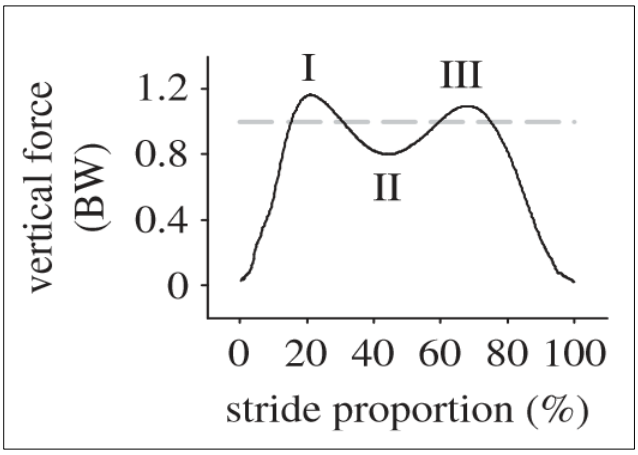

Figure 2-6. A plot of the vertical GRF during the stance phase of walking. The GRF is normalized by subject body weight. Foot-ground contact is characterized by an impact phase (I), a vault phase (II), and a propulsive phase (III). The dashed line represents 1 BW (Usherwood et al., 2012).

the propulsive phase (III), the vertical GRF increases and is shifted anterior to the ankle. The vertical GRF is coupled with the force produced by the ankle plantarflexors to make the foot a stiff lever suited for toe push-off, which subsequently enables the storage and release of elastic energy in the Achilles tendon.

Piazza & Delp (1996) analyzed the swing leg during walking with a musculoskeletal model of the lower extremity (Figure 2-7). The simulation calculated the hip, knee, and ankle angle during the swing phase, which utilized published experimental data of the kinetics and kinematics of human walking and EMG of lower-extremity muscles. A systematic variation of muscle excitation during each time step of the analysis revealed that a decrease in peak knee flexion resulted from a decrease in hip flexion moment, an increase in hip angular velocity at toe-off, and a decrease in knee angular velocity at toe-off (Piazza and Delp, 1996). Interestingly, Piazza and Delp (1996) found that the gastrocnemius produces a knee extension moment during a portion of the swing phase due to two-body pendulum dynamics. If the ankle plantarflexor moment is greater than the knee flexion moment, then it results in a net knee extension moment. The knee is accelerating to extension throughout the entire simulation due to a combination of centrifugal, coriolis, and gravitational forces (Piazza and Delp, 1996).

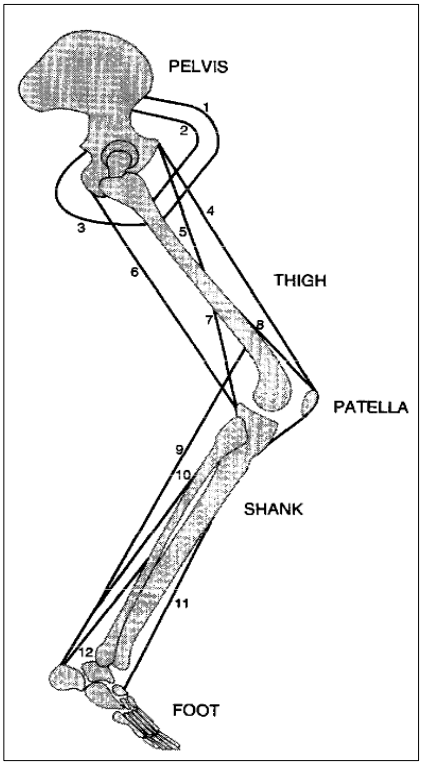

Figure 2-7. The lower extremity model of the swing leg during walking. The model consisted of a pelvis, thigh, patella, shank, foot, and twelve muscles that spanned the joints (Piazza and Delp, 1996).

2.3.2 Measure of Stability

The most common interpretation of human gait stability during walking is the capacity to walk without falling. Formally, stability is defined by the method by which it is measured. Rosenblatt and Grabiner (2010) discussed three methods of measuring gait stability during walking: step width (SW), step width variability (SWV), and margin of stability (MOS). The authors suggested that SW and SWV are measures of lateral stability and MOS is a measure of dynamic stability. The MOS was a percentage of the total time that the whole-body center of mass is directly above the body's base of support. Dynamic stability increase as the MOS increases. The margin of stability was at its lowest during heel strike due a small base of support. Lateral stability was directly proportional to SW and inversely proportional to SWV. Rosenblatt and Grabiner (2010) captured the motion and GRF of subjects walking on a treadmill and overground at varying speeds. The SW, SWV, and MOS did not vary significantly with walking speed. The authors reported that SW and SWV varied across the walking tasks, but the MOS did not vary. Step width was greatest for treadmill walking ($p = 0.001$) and SWV was greatest for overground walking ($p = 0.001$). Rosenblatt and Grabiner (2010) suggested that the MOS of stability did not significantly change between walking speeds or walking trials because foot placement was consciously monitored by the subject.

Schablowski and Gerner (2006) discussed two methods of measuring dynamic stability during human walking: Floquet multipliers (FMs) and local divergence exponents (LDEs). Floquet multipliers and LDEs are a measure of orbital and local stability, respectively. Schablowski and Gerner (2006) captured the lower extremity

kinematics of ten subjects walking at speeds from 0.2-1.4 m/s in increments of 0.2 m/s for 90 seconds. The authors then modeled the state space on a Poincaré map to find small oscillations within the state space. Schablowski and Gerner (2006) reported that dynamic stability of one step, as measured by FMs, is highest at walking speeds between 1.0 and 1.2 m/s. The authors reported that dynamic stability was also dependent upon the time scale. That is, period-one stability was highest at different walking speeds compared with stability over multiple steps. The examination of LDEs revealed that short-term dynamic stability for one step was maximized between 1.0 and 1.2 m/s, but that long-term dynamic stability (over four steps) decreased as the speed increased (Figure 2-8).

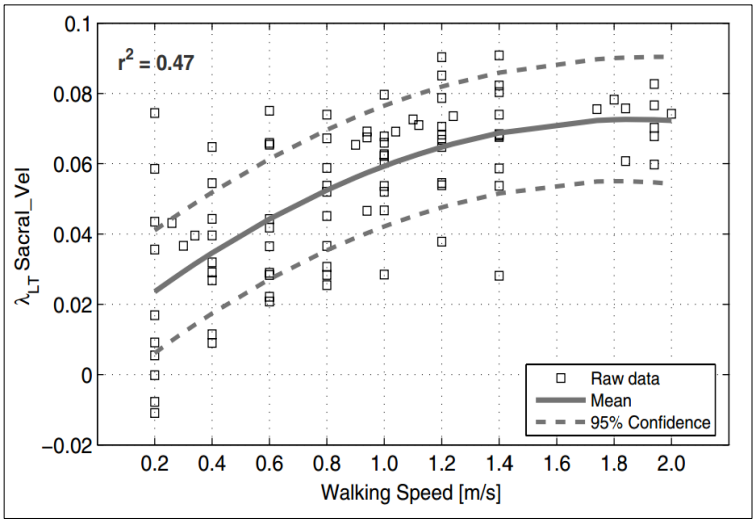

Figure 2-8. A plot of the average sacral (velocity) long-term LDE, λ_{LT}, for varying walking speeds of ten subjects. The LDE value is inversely related to stability. LDE values less than zero are dynamically stable (Schablowski and Gerner, 2006).

Dingwell and Kang (2006) examined the relationship between orbital and local stability during human walking using FMs and LDEs, respectively. Dingwell and Kang (2006) captured lower extremity kinematics and trunk accelerations of ten subjects on a level treadmill and walking on a flat 200-meter track at a subject-selected, comfortable walking speed. The authors found that their subjects were orbitally stable during both overground and treadmill walking, but were not locally stable. Dingwell and Kang (2006) found no correlation between orbital and local stability. The state trajectory of a

body segment was recorded for multiple steps. Each step represented one cycle and the mean state trajectory of all of the cycles was calculated. Dingwell and Kang (2006) reported that the state trajectory would converge to the mean state trajectory, which is indicative of stable walking in terms of orbital stability. However, the state trajectory of neighboring cycles diverge, which is indicative of unstable walking in terms of local stability. It was not clear to the extent at which a human can be unstable locally and remain stable globally.

There are many different methods to quantify dynamic stability, but the short list discussed here include measuring step width, step width variability, margin of stability, Floquet multipliers, and local divergence exponents. Step width, step width variability, margin of stability, Floquet multipliers, and local divergence exponents can be quantified using force plate readings or motion data. Floquet multipliers and local divergence exponents measure orbital and local stability, respectively. The definition of stability is dependent upon the methods used to measure it. This is important to note because stability measurement are not necessarily correlated. That is, a mechanical system or person can be simultaneously stable in one aspect while simultaneously unstable in another.

2.4 Soft Tissue and Ground Contact

2.4.1 Soft Tissue

Human body segments are typically modeled as rigid bodies during locomotion despite the fact that the majority of human mass is made up of soft tissue (Clarys et al., 1986). Mechanical energy entering the dynamic system at initial foot contact could potentially be dissipated by soft tissue vibration. Pain and Challis (2002) determined that an increase in soft tissue stiffness increased the loading rate and peak of the ground reaction force during vertical arm strikes. Furthermore, soft tissue varies in stiffness and the underlying tissues may be oscillating at varying frequencies. Energy may be dissipated through friction between the underlying tissues that make up the mechanical system.

Clarys et al. (1986) dissected three male and female cadavers to validate the use of *in vivo* anthropometric measurements as an estimate of underlying tissue masses. The cadavers were each partitioned into 14 segments: hand (2), forearm (2), arm (2), foot (2), shank (2), thigh (2), head, and torso. Each segment was weighed with a balance beam and underwater with a Mettler Precision Scale. The skin, adipose tissue, muscle, and bone were separated. The mass, volume, density, and percentage of segment mass were calculated for each tissue type. The tissue parameters were compared with regression models based on anthropometric measurement described by Marfell-Jones (1984). The only measurement that had a correlation coefficient lower than 0.66 were skin tissue mass, hand adipose tissue mass, and foot adipose tissue mass (Clarys et al., 1986). The majority of the other parameters had a correlation greater than 0.80. Due to the focus of

this thesis, it is important to note that the percent of the segment mass that was identified as soft tissue was 90.3% and 77.6% for the thigh and shank, respectively (Clarys et al., 1986).

Pain and Challis (2002) analyzed forearm soft tissue displacement during repetitive vertical, downward strikes onto a force plate. The subject struck the force plate with the palmar aspect of the hand with the forearm musculature relaxed, moderately tensed, and fully tensed a total of nine times for each condition. The position of 28 markers fixed to the anterior forearm and the ground reaction forces were recorded. Furthermore, the markers were partitioned into 18 sectors to analyze the change in area. The mean peak vertical ground reaction force for the relaxed and fully tensed conditions were not significantly different ($p>0.01$). The sector area changes were 100% greater for the relaxed condition compared with the fully tensed condition for all 18 sectors. The mean change in area for the relaxed condition was 11%. The sector areas and marker positions post impact were characteristic of a damped sinusoidal wave (Figure 2-9. A representative vertical marker displacement following impact with a force plate. This marker was attached to the anterior aspect of the forearm (Pain and Challis, 2002).). Pain and Challis (2002) reported the lag time in response to impact between the proximal and distal markers to be 4.2 milliseconds.

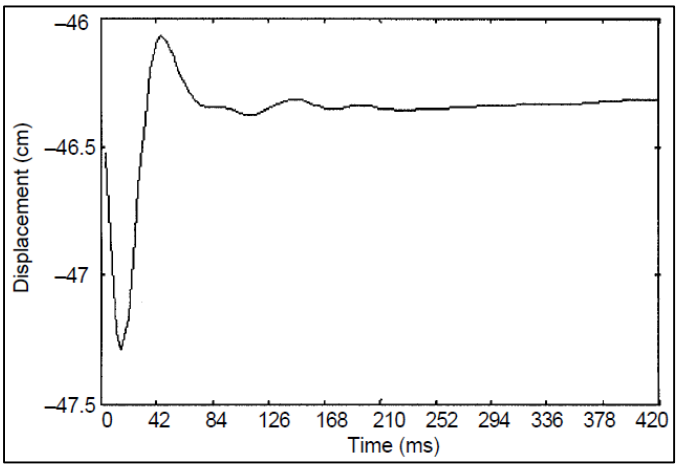

Figure 2-9. A representative vertical marker displacement following impact with a force plate. This marker was attached to the anterior aspect of the forearm (Pain and Challis, 2002).

These results indicated that the energy transmitted via soft tissue vibration was not negligible. Roughly 70% of dissipated energy immediately following impact was due to the soft tissue vibration (Pain and Challis, 2002). The difference in marker displacement between the relaxed and fully tensed conditions were most likely due to changes in underlying muscular stiffness since palmar deformation and skin stiffness would have remained relatively constant (Pain and Challis, 2002).

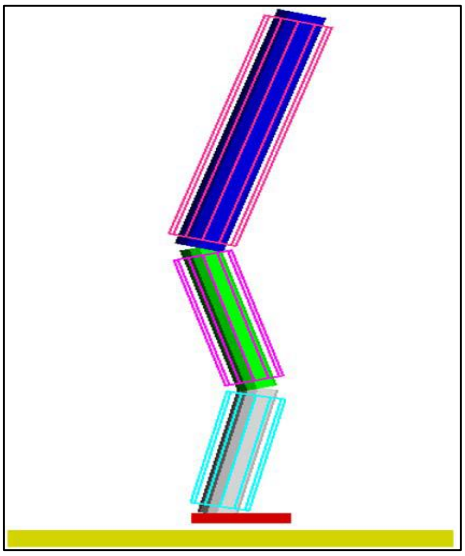

Figure 2-10. Computer simulated four-link wobbling model. The inner tubes represent hard tissue, and the outer tubes represent soft tissue. (Pain and Challis, 2006).

Pain and Challis (2006) measured the ground reaction force and soft tissue vibration of a subject during a 0.43-meter drop. Subject segment kinematics were measured in order to provide a means of evaluating a computer simulation of models with and without wobbling masses (Figure 2-10). The soft tissue oscillation of the subject's posterior shank and anterior thigh using the same protocol described in Pain and Challis (2002) to determine the frequency and amplitude of tissue vibration. The segment mass, center of mass location, moments of inertia, and soft tissue mass percentage were calculated for the model based on subject anthropometric parameters. The joint spring-damper actuator parameters were calculated so that the experimental and computer simulated ground reaction force curve matched for the wobbling mass model. The fully rigid model ground reaction force and joint torques were calculated to match the experimental kinematics of the drop. Pain and Challis (2006) found that the difference

between the experimental and wobbling model kinematics were less than or equal to 1° for the shank and 4.5° for the thigh. The peak torque and force at each articulation was greater for the rigid model compared with the wobbling model (Table 2-1. Peak joint torques and forces of following impact with the ground from a 0.43 meter vertical drop (Pain and Challis, 2006).). The peak ground reaction forces for the subject, wobbling model, and rigid model were 1640, 1620, and 4050 percent of the total bodyweights, respectively (Pain and Challis, 2006). Furthermore, the ground reaction force profile of the wobbling model was within 12% of the first 40 milliseconds and 5% of the first 15 milliseconds following impact (Pain and Challis, 2006). These results indicate that the wobbling model was a better predictor of impact ground reaction forces and joint kinetics compared with a fully rigid model.

Table 2-1. Peak joint torques and forces of following impact with the ground from a 0.43 meter vertical drop (Pain and Challis, 2006).

Joint	Wobbling mass model		Rigid body model	
	Torque (Nm)	Vertical force (N)	Torque (Nm)	Vertical force (N)
Ankle	−228	11080	−370	17140
Knee	267	7720	500	13280
Hip	−240	5100	−460	7700

Zelik and Kuo (2010) indirectly evaluated the contribution of soft tissue deformation to energy dissipation during walking. Ten subjects walked on a treadmill at systematically increased walking speeds between 0.7-2.0 m/s. The kinematics and ground reaction forces of each subject were collected and analyzed over a forty second interval. The joint work at the hip, knee, and ankle were calculated using inverse dynamics for each stride and averaged between subjects. Furthermore, the work calculated from the center of mass (COM) energy of each segment was computed and

averaged across subjects. Zelik and Kuo (2010) found that the total work calculated using traditional inverse dynamics methods increased as treadmill speed increased (Figure 2-11). In contrast, the total work calculated via the COM of each segment slightly decreased for all treadmill speeds (Zelik and Kuo, 2010). It was also reported that the negative COM work directly proceeding collision was more than 300% greater than the joint work. Zelik and Kuo (2010) determined that the traditional inverse dynamic method for measuring joint work does not account for negative joint work. This indicated that the forces due to soft tissue deformation, which was not accounted for during traditional inverse dynamic analysis, did negative work directly following ground contact and dissipated energy during walking.

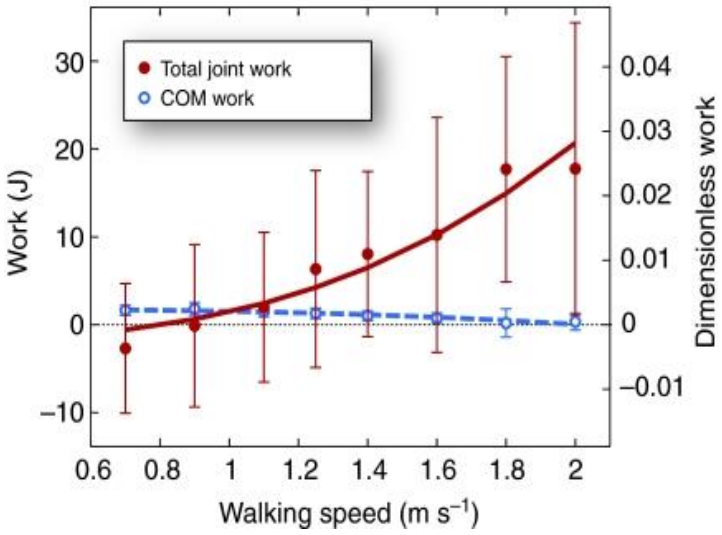

Figure 2-11. The summation of joint work calculated using traditional inverse dynamics and COM work for varying walking speed (Zelik and Kuo, 2010).

The vast majority of human mass is made up of soft tissue. Traditional inverse dynamic analysis does not account for soft tissue vibration. There is conclusive evidence that soft tissue vibration is a non-negligible phenomena resulting from energy transfer during human locomotion. Results from multiple studies suggest that inclusion of soft tissue oscillation following heel-ground contact in computer simulations produce more characteristic kinematic profiles (Pain and Challis, 2002; Pain and Challis, 2006; Zelik

and Kuo, 2010). Currently, passive-dynamic walkers have many kinematic similarities to human walking and are sensitive to external forces. The addition of wobbling masses to a passive-dynamic walker may decrease the sensitivity of the walker to perturbations from the environment, thus increasing its stability.

2.4.2 Modeling Impact and Elastic Contact

Blickhan (1989) modeled human locomotion with a simple, classic approach often used in biomechanics – a spring-mass model. The model presented in Blickhan (1989) consisted of a rigid mass supported by a massless spring. This model is most often used to study hopping and running. Blickhan (1989) derived the equations for the contact phase and flight phase of the spring-mass model. The author simulated running by "hopping forward" with a similar spring-mass model. An important finding reported by Blickhan (1989) was that an infinite number of trajectories were possible when all the parameters of the model were held constant and only the landing speed and stiffness of the spring were changed. Similar to hopping, the model could correctly predict running gait characteristics. This model, although not a comprehensive or thorough tool for analyzing human locomotion, is an example of the usefulness of a simple model for analyzing the ground contact during human locomotion.

Zadpoor and Nikooyan (2010) developed a spring-mass-damper model to simulate the ground reaction force during running. This model included four of the following: masses, springs, and dampers. The masses of the system included a wobbling and rigid masses for both the upper and lower body. In this model, the authors optimized

the spring stiffness and damping coefficients of the lower-body wobbling mass to minimize its oscillation. The authors varied the surface stiffness and damping. Zadpoor and Nikooyan (2010) reported that the peak ground reaction force during initial loading remained constant as the surface properties changed. The results found by Zadpoor and Nikooyan (2010) indicated that the stiffness of the lower leg was important in determining the ground reaction force experienced for different surfaces. When the lower-body wobbling mass stiffness was not optimized, the peak ground reaction force increased as the stiffness of the surface increased. Increased muscle activity was a means to increase underlying soft tissue stiffness during forearm strikes (Pain and Challis, 2002). It may be that a role of muscular activity during human locomotion is to regulate underlying tissue stiffness and compensate for varying ground stiffness.

Qi et al. (2011) introduced an elastic contact between the feet and ground of planar passive-dynamic walkers in two dimensions. Each leg of the passive walker was represented by one rigid body with round feet. The parameters of the model were leg length, leg mass, leg moment of inertia, leg center of mass, and ramp incline. The contact surfaces followed a Hertz contact model and Coulomb friction model. The Hertz contact law was used to estimate the ground reaction force normal to the contact surfaces, which included both nonlinear spring and damping components. The Coulomb friction law estimated the ground reaction force parallel to the contact surfaces, which was dependent upon the relative velocity of the foot in contact with the ground and coefficient of friction. Qi et al. (2011) found that the passive-dynamic walker was unaffected by high damping coefficients, but at low damping coefficients the passive-dynamic walker could not sustain locomotion. Qi et al. (2011) also found that coefficients of friction less

than or equal to 0.3 for static friction and 0.2 for dynamic friction caused the swing leg to slip during contact with the ground. Qi et al. (2011) reported that a major determinant of walking gait was contact stiffness. It was not surprising that as the contact stiffness decreased, the normal ground reaction force and walking speed decreased as well.

2.5 Summary

Passive-dynamic walkers have been utilized in many different forms to study human walking. Passive-dynamic walkers are inherently sensitive to modifications of the model configuration and initial conditions, and therefore provide a great tool in studying the effects of the different components on human walking gait. Human walking has been studied extensively since the 1800's. However the majority of models that represent the human body are a series of linked rigid bodies without a soft tissue component. The vast majority of the human body is made up of soft tissue that vibrates during human locomotion. Soft tissue vibration has been shown to dissipate energy and decrease the mechanical loading at the joints. A soft tissue component may affect the dynamics of a bipedal walker such that the gait cycles become more dynamically stable and robust to perturbations of the environment; this will be the focus of subsequent chapters.

Chapter 3

Methods

3.1 Introduction

The methods section will discuss the mathematical modeling of passive-dynamic walkers, and the stability analyses performed on the motion of these walkers. The test model consisted of both rigid body components and a soft tissue component. The soft tissue component was modeled as a mass-spring-damper system that stored and dissipated energy during the gait cycle. The control model was mechanically the same model, except it lacked a soft tissue component. Comparisons of the two models allowed assessment of the role of the soft tissue model component (oscillating mass) on model gait stability. Section 3.1.1 will outline the nomenclature that will be used in the following sections and subsections. Section 3.1.2 will describe the mathematical model of the PDWs. Section 3.1.3 will give the simulation details for the following stability measurements. Section 3.2.1 to Section 3.2.4 will outline the methods for the stability measurements calculated.

3.2 Simulation Overview

3.2.1 Nomenclature

Symbol	Name	Value
M	Hip Mass	10 kg
m	Foot Mass	1 kg
l	Leg Length	1 m
g	Gravity	9.81 m/s^2
β	Incline Angle	Varies (rad)
t	Time	Varies (sec)
$\varphi_1(t)$	Stance Leg Angle (rad)	Varies (rad)
$\varphi_2(t)$	Swing Leg Angle	Varies (rad)
$\phi_1(t)$	Stance Leg Ang. Velocity	Varies ($rad.s^{-1}$)
$\phi_2(t)$	Swing Leg Ang. Velocity	Varies ($rad.s^{-1}$)
m_w	Oscillating Mass (OM)	1 kg
$x(t)$	OM horizontal position	Varies (m)
$y(t)$	OM vertical position	Varies (m)
k	Spring Stiffness	Varies ($N.m^{-1}$)
c	Damping Coefficient	Varies ($N.s.m^{-1}$)

3.2.2 Passive-Dynamic Walking Models

A two-dimensional passive-dynamic walker (PDW) was modeled to study the effects of soft tissue vibrations on gait dynamics. The PDW modeled in Garcia et al.

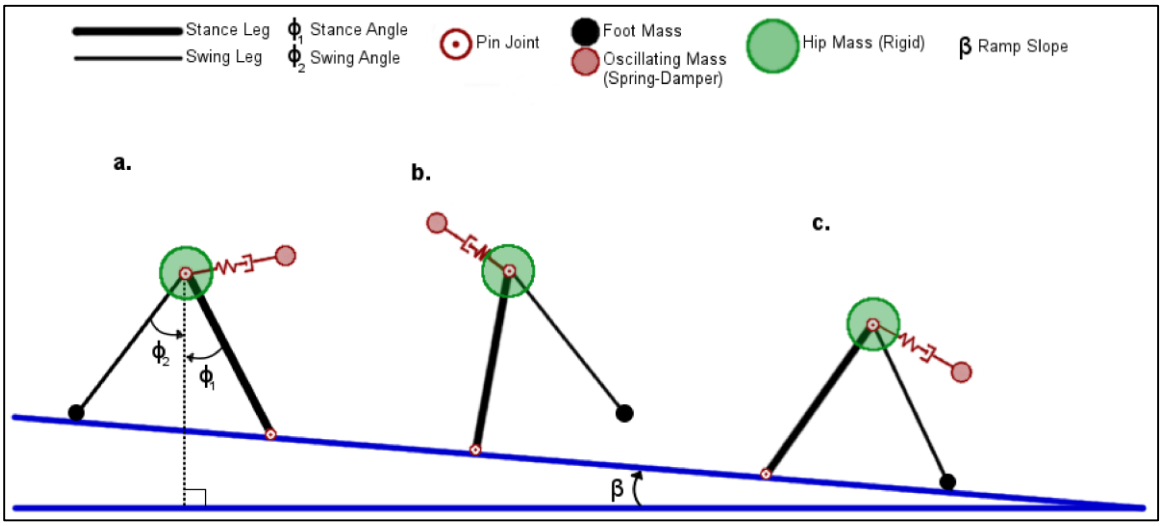

Figure 3-1. Diagram of a passive oscillating mass walker. (a) The initial position of a step cycle. (b) An intermediate position of a step cycle. (c) Foot ground contact at the end of a step cycle.

(1998) served as a control walker. The test walker was identical in every aspect except for the addition of a mass-spring-damper system attached at the hip joint. Both walkers consisted of two point masses (hip mass, *M*, and foot mass, *m*) connected to the ends of massless, rigid legs (Figure 3-1). One of the legs attached the hip mass to the ground by way of a revolute joint with a single degree of freedom located at the ground. The other leg attached the foot mass to the hip mass with one rotational degree of freedom. The joint was located at the center of the hip mass. The equations of motion for this system is that of a double pendulum,

$$\ddot{\varphi}_1(t)\left(1+2\,\frac{m}{M}\left(1-\cos\left(\varphi_1(t)+\,\varphi_2(t)\right)\right)\right)+\,\ddot{\varphi}_2(t)\frac{m}{M}\left(1-\cos\left(\varphi_1(t)+\,\varphi_2(t)\right)\right)$$

$$-\frac{m}{M}\left(\dot{\varphi}_2(t)^2-2\dot{\varphi}_1(t)\dot{\varphi}_2(t)\right)\sin\left(\varphi_1(t)+\,\varphi_2(t)\right)+\frac{m}{M}\frac{g}{l}\left(\sin\left(\varphi_2(t)\right)-\sin\left(\varphi_1(t)\right)\right)$$

$$-\frac{g}{l}\sin\left(\varphi_1(t)\right)=0$$

$$\ddot{\varphi}_1(t)\frac{m}{M}\left(1-\cos\left(\varphi_1(t)+\,\varphi_2(t)\right)\right)-\frac{m}{M}\ddot{\varphi}_2(t)\,+\frac{m}{M}\dot{\varphi}_1(t)^2\sin\left(\varphi_1(t)+\,\varphi_2(t)\right)+\frac{m}{M}\frac{g}{l}\sin\varphi_2(t)=0$$

For these simulations, the hip mass was assumed to be much more massive than the foot mass. That is, $\frac{m}{M} \approx 0$. This assumption simplified the equation of motion for the stance leg (φ_1) to an inverted pendulum,

$$\ddot{\varphi}_1(t) = \sin \varphi_1(t) \tag{1}$$

Where time in Equation (1) and all following equations of motion was scaled by *g/l*. The equation of motion for the swing leg (φ_2) was,

$$\ddot{\varphi}_2(t) = \ddot{\varphi}_1(t) + \dot{\varphi}_1(t)^2 \sin(\varphi_1(t) + \varphi_2(t)) \tag{2}$$
$$- \cos \varphi_1(t) \sin(\varphi_1(t) + \varphi_2(t))$$

The equation of motion for Equation (2) is that of a simple pendulum where the hinge attachment is following the trajectory of an arc. Due to the geometry of the PDW, foot-ground contact occurred when the following equation was satisfied,

$$\varphi_1(t) - \varphi_2(t) + 2\beta = 0 \tag{3}$$

Equation (3) was satisfied at two instances of the gait cycle. One instance occurred when the swing leg was collinear to the stance leg. This instance was ignored to allow the swing foot to pass through mid-stride. The second instance was not ignored and indicated a transfer of the hip mass from the pre-collision stance leg to the post-collision stance leg at the instant of foot-ground contact. The transfer of swing-to-stance and stance-to-swing was instantaneous and the force applied to the new swing leg during the transition was assumed to be impulsive. This required that the angular momentum was conserved from pre- to post-collision. At foot-ground contact, the magnitude of the stance leg angle and swing leg angle were the same pre- and post-collision, and the post-collision angular velocities were calculated by fulfilling the requirement for the

conservation of angular momentum. The jump condition from the final state of a gait cycle to the initial state of the following cycle was calculated as,

$$\varphi_1^+ = -\varphi_1^- \tag{4}$$

$$\dot{\varphi}_1^+ = \dot{\varphi}_1^- \cos 2\varphi_1^-$$

$$\varphi_2^+ = -\varphi_1^-$$

$$\dot{\varphi}_2^+ = \dot{\varphi}_1^+ (1 - \cos 2\varphi_1^+)$$

The "-" superscript denotes the position/velocity pre-foot-ground contact, and the "+"superscript denotes position/velocity post-foot-ground contact.

The addition of an oscillating mass to the hip required a modification of the equation of motion for the stance leg (5) and the addition of two equations of motion to prescribe the motion of the oscillating mass (6)-(7).

$$\ddot{\varphi}_1(t) = \sin\varphi_1(t) - \frac{l\cos\varphi_1(t)\ [k\,x(t) + c\,(\dot{x}(t) + \dot{\varphi}_1(t)\cos\varphi_1(t))]}{M\,g} - \frac{l\sin\varphi_1(t)\ [k\,y(t) + c\,(\dot{y}(t) + \dot{\varphi}_1(t)\sin\varphi_1(t))]}{M\,g} \tag{5}$$

$$\ddot{x} = -l\,\frac{k\,x(t) + c\,(\dot{x}(t) + \dot{\varphi}_1(t)\cos\varphi_1(t))}{m_w\,g} \tag{6}$$

$$\ddot{y} = -l\,\frac{k\,y(t) + c\,(\dot{y}(t) + \dot{\varphi}_1(t)\cos\varphi_1(t))}{m_w\,g} \tag{7}$$

Where x was the position in the horizontal direction and y was the position in the vertical direction relative to the hip mass. The spring-damper parameters were denoted by k, the spring stiffness, and c, the damping coefficient. The equation of motion for the swing leg remained unaltered.

A fixed point for the equations of motion was an initial state that resulted in an identical initial state for the following step. That is to say,

$$\boldsymbol{F}(\boldsymbol{q}^*) = \boldsymbol{q}^* \tag{8}$$

Where $\boldsymbol{q^*}$ is the fixed point state of the system and $\boldsymbol{F(q^*)}$ is the mapping function. Garcia et al. (1998) derived an analytical solution that approximated fixed points for small slopes for the control walker modeled in equations (1)-(4). Due to equation (3) prescribing the final state of the system, the analytical solution could be reduced to the state of the stance leg. That is, fixed points of equations (1)-(2) were only dependent upon the state of the stance leg. These fixed points were found numerically by systematically incrementing the damping and stiffness coefficients and allowing the gait cycle of the walker to converge to a period-n gait. When all the fixed point values were located, they were plotted into bifurcation diagrams (damping was held constant and stiffness was the bifurcation parameter) to visually inspect the system dynamics.

The PDWs were modeled and analyzed in MATLAB, which is a technical computing environment. Specifically, the differential equation solver used was *ode113*. *ode113* is a nonstiff solver that has high accuracy. This solver using a variable-order Adams-Bashforth-Moulton (ABM) method (Gear, 1971). The ABM method also utilizes

an adaptive step time. The method takes into account the rate at which the system is changing for the preceding time steps. If the system is changing at a high rate, then the step time is small and vice versa. The precision of the machine was between $1x10^{-15}$ and $1x10^{-16}$. Therefore the precision of the integrator was tightened to allow absolute error up to $1x10^{-14}$.

Five measures were used to test stability: Floquet multipliers, local divergence exponents (LDEs) (also known as Lyapunov exponents), basin of attraction, slope perturbation range, and step time variability. Floquet multipliers measure step-to-step stability and LDEs measure inter-step stability. The basin of attraction and slope perturbation range measure the maximum state perturbation and slope perturbation, respectively, that can be applied to the walker without the walker falling over during the subsequent steps. The step time variability is a measure of the step variance for the walking on uneven terrain.

3.2.3 Simulation Details

Limit cycles were found for varying spring-damper parameters and slopes. Pilot simulations revealed that fixing the damping values and incrementing the stiffness values to find limit cycles was the most efficient approach. The alternative approach was computationally heavy because the differential equations became stiff as the damping values increased above 12 $N.s.m^{-1}$. Furthermore, damping above 12 $N.s.m^{-1}$ produced results that were overly complex in terms of the bifurcation dynamics, therefore outside of the scope of this research. The damping values analyzed were between 0-12 $N.s.m^{-1}$ in

increments of 0.25 $N.s.m^{-1}$. The spring stiffness values were incremented by 0.1 $N.m^{-1}$ (starting at 0 $N.m^{-1}$) until the PDW failed. Failure was detected when the PDWs hip mass made contact with the ground before the foot mass made contact with the ground, that is, the walker fell over. Some examples of the initial conditions of the stance leg that resulted in period-1 gait cycles can be found in Table 3-1.

Unless specified otherwise, simulations were run for 200 steps, or until the model failed. Pilot simulations revealed that 200 steps was beyond a sufficient number of steps to reach a level of convergence (of a limit cycle) below a tolerance of $1x10^{-12}$ rad and $1x10^{-12}$ $rad.s^{-1}$. The true fixed point of a period-1 gait cycle is at a level more precise than the machine accuracy. Therefore, the fixed point oscillates in the state space immediately surrounding the fixed point. The range of this state space was between $1x10^{-12}$ rad or $rad.s^{-1}$ and $1x10^{-13}$ rad or $rad.s^{-1}$. Therefore, the convergence criterion was established as the upper limit of that range. Unless specified otherwise, the slope for all analyses was 0.009 radians. Pilot simulations revealed that 0.009 radians was midrange in terms of the slope range for which the control walker ambulated.

The control PDW and oscillating PDW can converge to two different limit cycles (depending on the initial conditions). These limit cycles are termed short-period gait and

Table 3-1. The initial conditions of the stance leg for the control PDW and three oscillating PDWs that resulted in period-1 limit cycles. The incline of the ground for these period-1 limit cycles was 0.009 radians. The counter-clockwise direction was the positive direction, therefore a negative stance leg angular velocity moved the hip of the PDWs to the right in Figure 3-1.

	------Control------	----------Oscillating----------		
c [$N.s.m^{-1}$]	0	3.5	10.0	12.0
k [$N.m^{-1}$]	0	25.8	32.3	168.3
φ_1 [rad]	0.200317210433	0.239246172775	0.234905034805	0.267985998793
$\dot{\varphi}_1$ [$rad.s^{-1}$]	-0.199836607033	-0.222714555361	-0.221225463121	-0.248517591470

long-period gait. A short-period gait had a period that was relatively small compared to the long-period gait cycle. Furthermore the short-period gait has a much smaller range of motion (the short-period gait) at a lower walking velocity than the long-period gait. Only the long-period gait of the PDWs were considered for simplicity in the analyses. A large number of the limit cycles found were period-n, n>1. A period-n limit cycle is a limit cycle that repeats every n-th period. To simplify the analyses, only period-1 gait cycles were examined. Without varying the slope, the control PDW ambulated only in period-1 gait.

Once the most stable gait cycles were found (in terms of local divergence exponents and Floquet multipliers) for each damping value (and corresponding spring value), the slope of the ground was varied to study the effects of slope on the stability of the PDWs. Limit cycles were found for these spring-damper systems on all of the slopes the PDWs ambulated.

3.3 Measurement of Stability

The following sub-sections will describe the stability analysis and slope variation in more detail.

3.3.1 Floquet Multipliers

Floquet multipliers are a measure of orbital stability (Hilborn, 2000). That is to say, Floquet multipliers can be used to measure how a walker behaves from step-to-step. In Floquet theory, if a limit cycle is an attractor, then there is a region surrounding the limit cycle such that if the system's state started in that region, it would converge to the limit cycle as time approaches infinity. A gait cycle, in the context of a passive-dynamic walker, is the state trajectory throughout one step cycle. If a gait cycle is an attractive limit cycle, then the Floquet multiplier value would be less than unity (< |1|). A period-one gait cycle is a cycle that repeats itself every step. As a result, each state of the state trajectory is a fixed point. For simplicity, the fixed point analyzed for the walker was chosen to be the initial state of a limit cycle. The PDWs only took one step in this analysis to determine the step-to-step Floquet multiplier. The initial state, q_{n-1}, was perturbed from the fixed point and the expansion of the distance between the initial state of the subsequent step, q_n, and the fixed point was measured,

$$q_n - q^* = F(q_{n-1}) - F(q^*) \tag{9}$$

A linearization of the equation (9) resulted in,

$$\boldsymbol{q_n - q^*} = \left.\frac{d\boldsymbol{F}}{d\boldsymbol{q}}\right|_{\boldsymbol{q^*}} [\boldsymbol{q_{n-1} - q^*}] \quad (10)$$

The fixed points were perturbed by ±1x10^{-6} units (rad or rad.s^{-1}) to numerically estimate the Jacobian matrix in equation (10), and the eigenvalues of the matrix were computed. The largest eigenvalue was the Floquet multiplier for the corresponding fixed point. Floquet multipliers were found for all period-one gait cycles.

3.3.2 Local Divergence Exponents

Local divergence exponents (LDEs) are a measure of local stability (Hilborn, 2000). Local divergence exponents are measured in a fashion similar to Floquet multipliers, except that they account for the rate of divergence of a perturbed state trajectory relative to the limit cycle following a small increment in time,

$$\dot{\boldsymbol{\varepsilon}}(\boldsymbol{q_\varepsilon}, \boldsymbol{q^*}) = \left.\frac{d\boldsymbol{F}}{d\boldsymbol{q}}\right|_{\boldsymbol{q^*}} \boldsymbol{\varepsilon}(\boldsymbol{q_\varepsilon}, \boldsymbol{q^*}) \quad (11)$$

Where $\boldsymbol{q_\varepsilon}$ is the perturbed state and $\boldsymbol{\varepsilon(q_\varepsilon, q^*)}$ is the difference between the perturbed state and the fixed point. The eigenvalues of the Jacobian matrix in equation (11) were numerically estimated for the state space immediately surrounding the fixed point (Figure 3-2). The largest

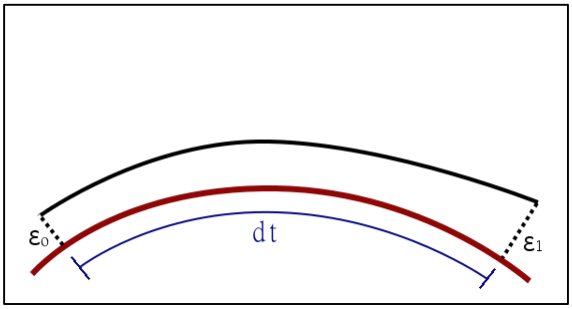

Figure 3-2. Diagram of a perturbed trajectory (black solid line) relative to the limit cycle trajectory (red solid line). The difference between the two trajectories is indicated by ε (black dotted line). The time period, dt (blue solid line), is very small. That is, dt << 1 sec.

eigenvalue of said estimated eigenvalues was considered the local divergence exponent. If the LDE was less than zero, then the system was stable. LDEs were estimated between 0-100% of one gait cycle in increments of 10%. The initial state of a gait cycle occurs at 0% of the gait cycle, and 100% of the gait cycle is the final state before foot-ground contact of the swing leg. The largest LDE was termed the "max LDE" and the average of all the LDEs over an entire stride was termed the "principal LDE." Local divergence exponents were estimated for all period-one gait cycles.

3.3.3 Basin of Attraction

The basin of attraction (BOA) is a measure of global stability. The BOA was the closed set of initial step conditions that converged to the fixed point (within $1x10^{-6}$ rad and $rad.s^{-1}$ of the stance leg position and velocity, respectively). The number of steps until the walker converged to the fixed point was recorded. The basin of attraction was numerically estimated for the control walker and oscillating mass walkers with varying spring-damper parameters. The parameters for the oscillating mass walkers were determined by the Floquet multiplier and LDE values. The optimal spring-damper parameters, in terms of stability, depended upon the mode of analysis. That is, the most stable parameters for the Floquet multiplier and LDE values did not coincide. Therefore, for each damping condition (0-12 $N.s.m^{-1}$ in increments of 0.25 $N.s.m^{-1}$), the optimal spring stiffness parameters were found according to the Floquet multiplier and LDE values. These spring-damper parameters were used for the BOA analysis.

The basin of attraction border search is illustrated in Figure 3-3. The initial search began at the fixed point (Figure 3-3a). The state space immediately surrounding the fixed point was analyzed to determine whether those initial states resulted in subsequent gait cycles that converged to the limit cycle of the fixed point or failed to converge (Figure 3-3b). The area surrounding the initial states that converged were then analyzed (Figure 3-3c-d) until the entire border of the basin of attraction was located. If the initial state converged, the number of steps to convergence were recorded. The search area was set to $1x10^{-12}$ $rad^2.s^{-1}$ to obtain high resolution data of the basin of attraction.

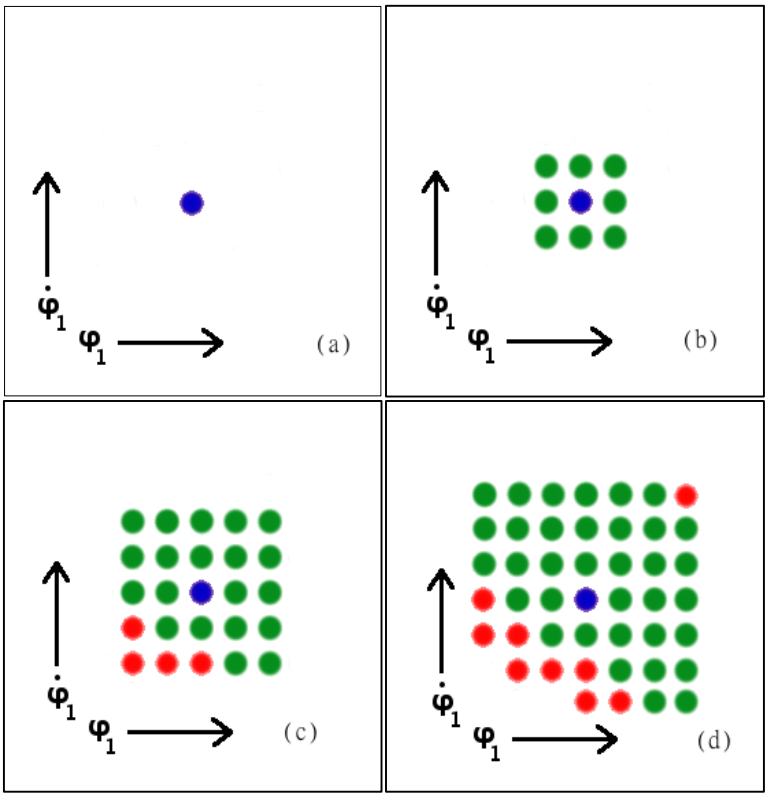

Figure 3-3. Diagram of the evolution of the basin of attraction border locator. (a) The fixed point locator begins at the fixed point, the blue dot, and (b) locates the convergence state space surrounding it, the green dots. (c & d) The convergent state space continues to grow until it approaches the border of the basin of attraction, the red dots. The horizontal axis is the initial stance leg position, and the vertical axis is the initial stance leg velocity.

3.3.4 Slope Perturbation Range and Step Time Variability

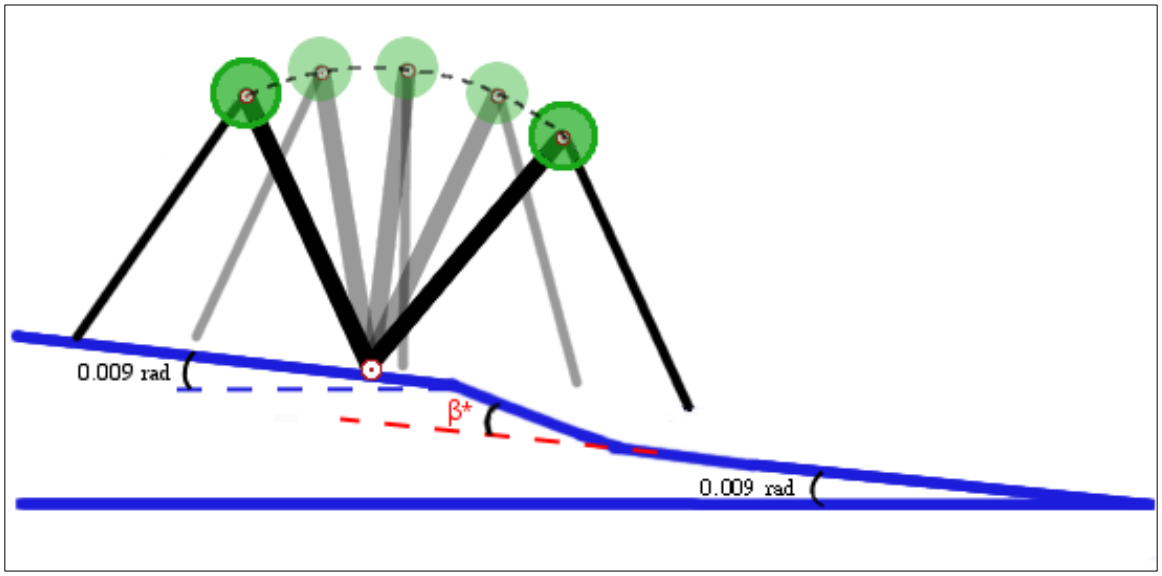

Figure 3-4. A diagram of a passive-dynamic walker and the perturbation of the slope during a step cycle. The perturbation, β*, is applied to a single step cycle. Subsequently, the passive-dynamic walker is simulated for 200 steps or until the walker fails. If the walker does not fail, the slope perturbation is incremented by ±0.002 radians.

During PDW ambulation, the slope was perturbed for a single period-1 step cycle (Figure 3-4). The initial conditions of the walker were chosen such that the walker started in a period-1 gait cycle. Therefore, the walker did not take any steps before the first perturbation. The subsequent 200 step cycles were recorded to detect if the PDW failed to ambulate. The slope for all subsequent step cycles was 0.009 radians. The slope perturbation was incremented +0.0002 radians until the walker failed to ambulate post-perturbation. For a further set of simulations, the slope perturbation was incremented by -0.0002 radians until the walker failed to ambulate post-perturbation. The range of slope perturbation values that did not result in PDW failure was termed the slope perturbation range (SPR). The SPR was found for all period-1 gait cycles for damping values between 0 $N.s.m^{-1}$ and 12 $N.s.m^{-1}$.

The control walker and the spring parameters for each damping condition that resulted in the largest SPR were analyzed further. The slope was randomly varied by a percentage of the control SPR (0.009 ±5-45%) for 200 steps. The control walker failed to ambulate for a total of 200 steps for percent values larger than 45% of the SPR. The step time variability (STV) was calculated as the standard deviation of the step time for all steps.

The same spring-damper conditions that were used to calculate the STV were utilized to calculate the range of slopes for which the oscillating PDWs could ambulate. The slope was systematically increased and decreased by 0.0001 radians until the walker failed to ambulate. For each slope condition, the slope was held constant and the walker took 200 steps. The range of slope values that the control PDW and oscillating PDWs could ambulate was termed *slope range* (SR). The Floquet multipliers and LDEs for the slope values that resulted in period-1 gait were calculated.

3.4 Summary

Two PDWs were simulated and their motion analyzed. The control PDW was a fully rigid body model with point masses at the feet and hip. The oscillating PDW contained the same components as the control PDW with the addition of a spring-mass-damper system that simulated soft tissue vibration. The spring-damper parameters of the oscillating PDW were varied systematically to study the effects of soft tissue vibrations on the stability of walking. Stability was tested by means of Floquet multipliers, local

divergence exponents, basin of attraction, step time variability, slope perturbation range, and slope range.

All stability measurements were estimated by way of numerical methods. All methods involved perturbing the parameters of the spring-damper system, the initial state conditions of a step, or the slope of the ground. The number of steps that the PDWs took until the gait cycle converged to the limit cycle, how quickly the gait cycle converged, or the variability of the gait cycle were recorded. These measurements served as the means for testing stability, and the effects of the spring-mass-damper system.

Chapter 4

Results

4.1 Introduction

The results of the mathematical modeling of passive-dynamic walkers, and the stability analyses performed on the motion of these walkers will be revealed in this chapter. Section 4.2.1 will describe the characteristics of the bifurcation diagrams with the spring stiffness as the bifurcation parameter. Section 4.2.2 and Section 4.2.3 will outline the analysis of local divergence exponents and Floquet multipliers, respectively. Section 4.2.4 will reveal the basin of attraction data. Section 4.2.5 contains the slope perturbation range, and step time variability results.

4.2 Stability Results

4.2.1 Bifurcation Diagrams

The bifurcation diagrams provide a means of visualizing the stability of a system. For example, the point at which a period-1 cycle bifurcates into a period-2 cycle is where the Floquet multiplier (FM) crosses unity. They also provide a means of predicting where another attracting limit cycle may exist due to a discontinuity in the graph. Furthermore, they serve as a general tools that help guide the stability analysis. It is easier to set up an analysis if the general behavior of the system is known.

The bifurcation diagrams grew and mutated as the spring-damper parameters were varied. In this section, *subcritical* and *supercritical* bifurcations will be discussed. A subcritical bifurcation is a discontinuous bifurcation. A supercritical bifurcation is a continuous, smooth bifurcation. In general, as the damping coefficient was increased, the range of stiffness values that produced stable walking increased. In all cases, the damping coefficient was held constant and spring stiffness was the bifurcation parameter. The complexity of the bifurcation diagrams ranged from relatively simple to highly nonlinear (and discontinuous). Characteristically, some of the bifurcation diagrams were very similar, therefore they will be discussed in groups. The groups, based on damping coefficients, were as follows: 0 N.s.m^{-1}, 0.5-3 N.s.m^{-1}, 3.5-8.5 N.s.m^{-1}, 9.0-10.5 N.s.m^{-1}, 11.0-11.5 N.s.m^{-1}, and 12.0 N.s.m^{-1}.

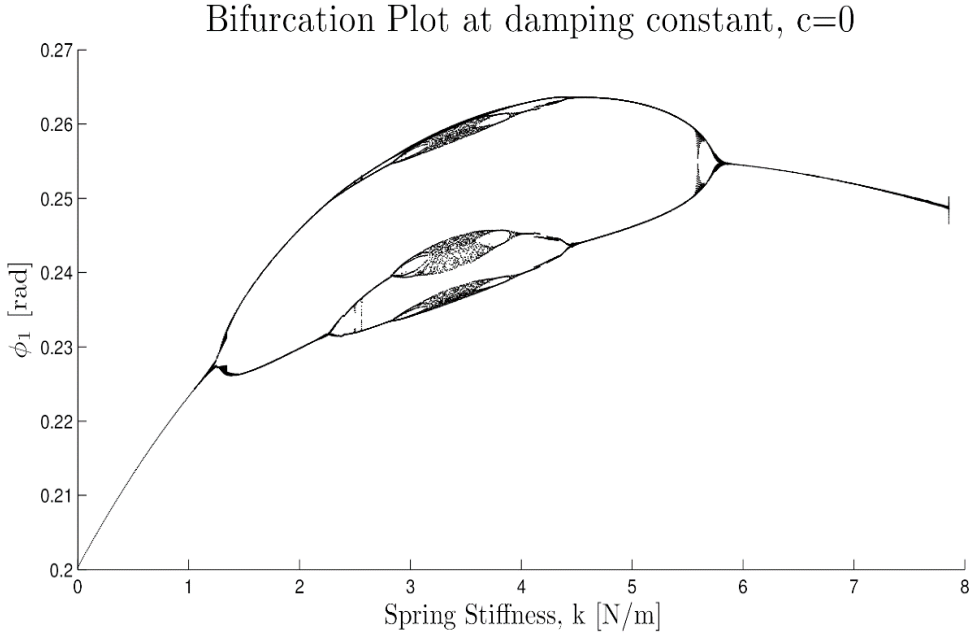

Figure 4-1. Bifurcation diagram at a damping coefficient of 0 N.s.m^{-1}. This diagram plots the bifurcation of the stance leg angle, φ_1, against the bifurcation parameter, spring stiffness. The maximum spring stiffness is 7.9 N.m^{-1}.

At no damping (Figure 4-1), the nonlinearity of the dynamics were in part due to the spring-mass system (*in part* because the dynamics of the walker are nonlinear without the spring-mass-damper system). As the spring stiffness increased, the gait-cycle evolved through a series of three period-doubling events (period-1 → period-2 → period-4 → period-8), then chaotic gait. Chaotic gait appeared at stiffness values around 3.25 $N.m^{-1}$. Chaotic gait was followed by a series of period-halving (period-8 → period-4 → period-2 → period-1). The walker ambulated at period-1 gait as spring stiffness increased until the walker failed (approximately 7.9 $N.m^{-1}$).

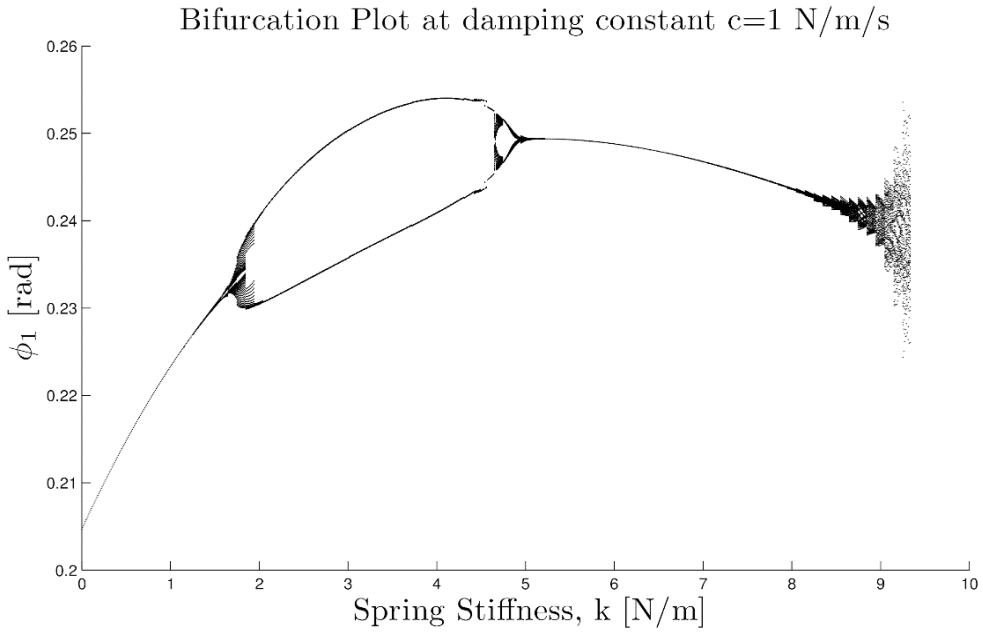

Figure 4-2. Bifurcation diagram at a damping coefficient of 1 $N.s.m^{-1}$. This diagram plots the bifurcation of the stance leg angle, φ_1, against the bifurcation parameter, spring stiffness. The maximum spring stiffness is 9.4 $N.m^{-1}$.

At the introduction of damping (0.5-3 $N.s.m^{-1}$), some of the bifurcations became discontinuous (Figure 4-2). Furthermore, the damping eliminated, in part, the chaotic gait that appeared at stiffness values around 3.25 $N.m^{-1}$. The range of stiffness values slightly increased relative to the 0 $N.s.m^{-1}$ condition, but the walker ambulated in a

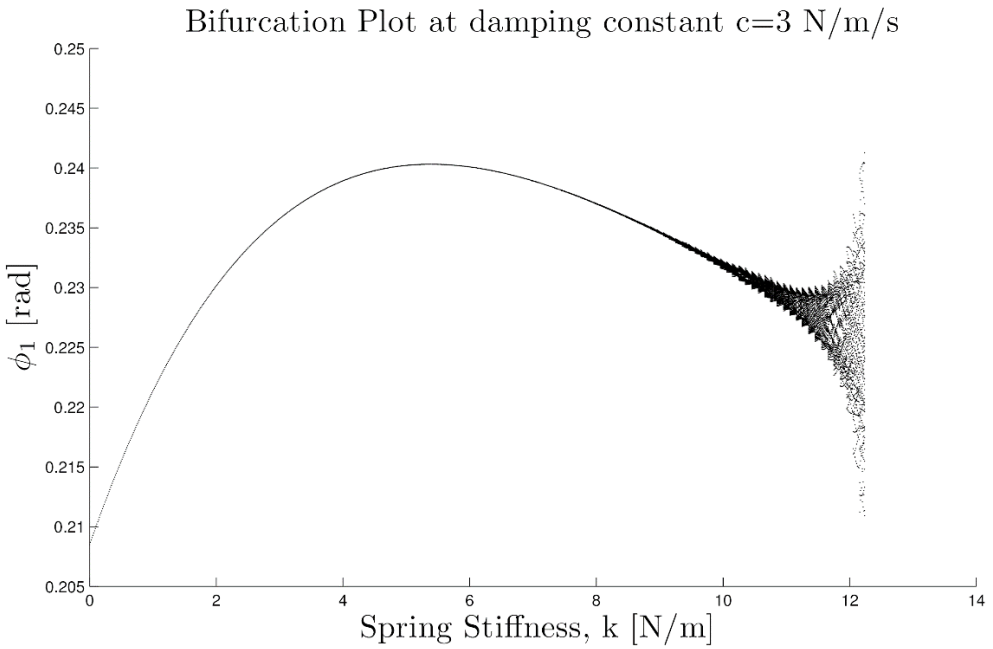

Figure 4-3. Bifurcation diagram at a damping coefficient of 3.0 N.s.m^{-1}. This diagram plots the bifurcation of the stance leg angle, φ_1, against the bifurcation parameter, spring stiffness. The maximum spring stiffness is 12.4 N.m^{-1}.

chaotic fashion beyond the largest stiffness value at no damping (i.e., when the stiffness value was larger than approximately 7.9 N.m^{-1}). At a damping value of 0.5 N.s.m^{-1}, the first bifurcation was period-doubling, but was quickly followed by a series of subcritical bifurcations (i.e., discontinuous bifurcations). The subcritical bifurcations resulted in a chaotic-like gait. A visual inspection estimated this period to be approximately period-32. This gait was very brief, because another series of subcritical bifurcations resulted in prolonged period-2 gait to period-1 gait, then brief chaotic walking until failure. As damping increased to 3 N.s.m^{-1} (Figure 4-3), the supercritical and subcritical bifurcations at low stiffness values disappeared and the range of stiffness values where the PDW ambulated increased. The chaotic walking at higher stiffness values was due to a rapid series of subcritical bifurcations until the walker failed.

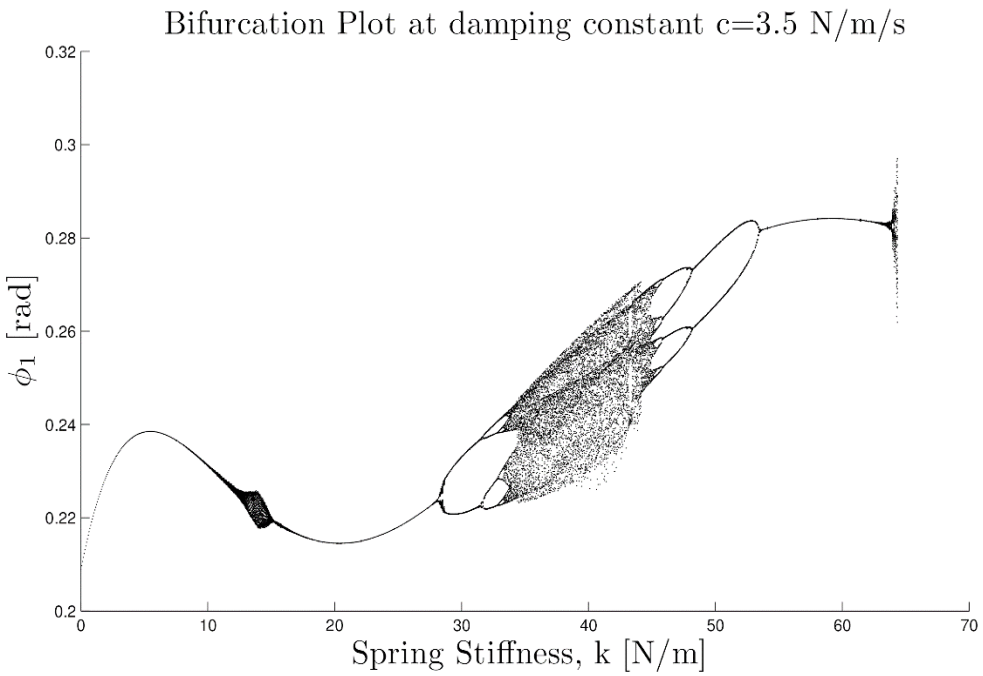

Figure 4-4. Bifurcation diagram at a damping coefficient of 3.5 N.s.m^{-1}. This diagram plots the bifurcation of the stance leg angle, φ_1, against the bifurcation parameter, spring stiffness. The maximum spring stiffness is 65.0 N.m^{-1}.

At damping values above 3 N.s.m^{-1} (Figure 4-4), a large change in the bifurcation diagram occurred. This change was due to a very large increase in the range of stiffness values for which ambulatory gait was found. The chaotic behavior that resulted in failure at a damping value of 3.0 N.s.m^{-1} can be observed in the bifurcation diagram at a damping value of 3.5 N.s.m^{-1}. Although, that chaotic behavior was followed by subcritical, period-halving bifurcations that resulted in period-1 gait. This period-1 gait was followed by a series of subcritical and supercritical period-doubling bifurcations (period-1 → period-2 → period-4 → period-8), then chaotic behavior. The chaotic gait was followed by supercritical period-halving bifurcations to prolonged period-1 behavior, which was followed by brief chaotic behavior before failure at a spring stiffness value of

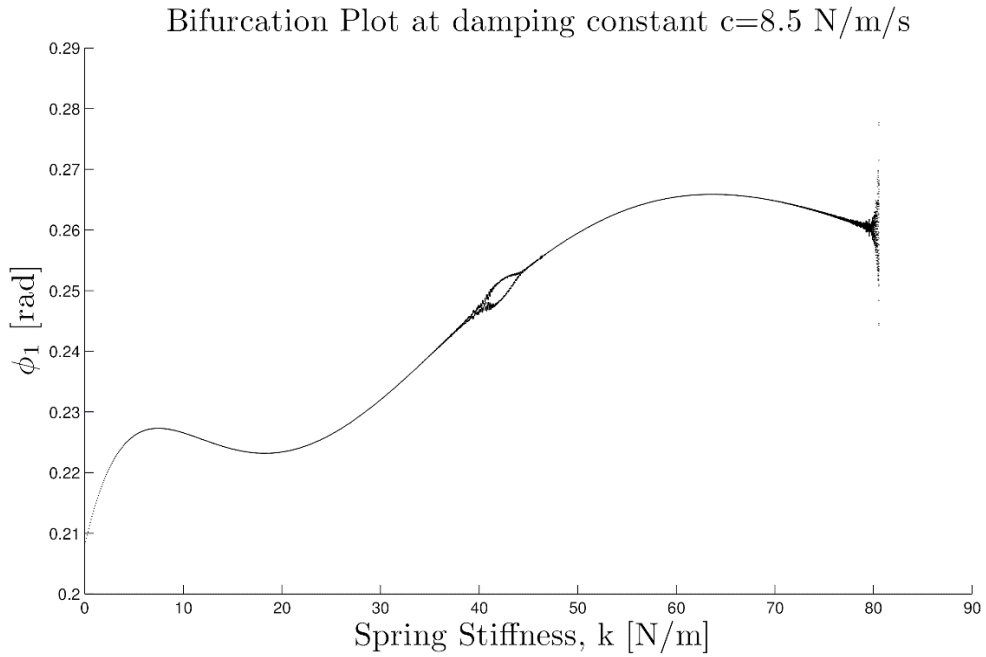

Figure 4-6. Bifurcation diagram at a damping coefficient of 8.5 N.s.m^{-1}. This diagram plots the bifurcation of the stance leg angle, φ_1, against the bifurcation parameter, spring stiffness. The maximum spring stiffness is 82.0 N.m^{-1}.

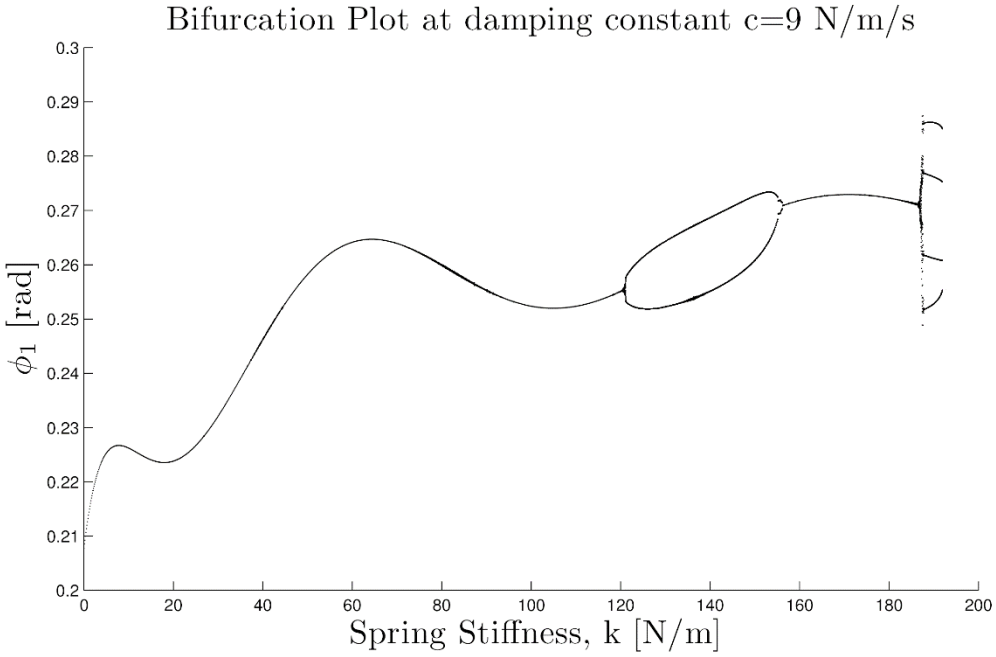

Figure 4-5. Bifurcation diagram at a damping coefficient of 9 N.s.m^{-1}. This diagram plots the bifurcation of the stance leg angle, φ_1, against the bifurcation parameter, spring stiffness. The maximum spring stiffness is 195.0 N.m^{-1}.

approximately 65-75 N.m^{-1}. As damping increased in 5 N.s.m^{-1}, the chaotic behavior between 10-15 N.m^{-1} disappeared. As damping increased to 8.5 N.s.m^{-1}, the supercritical bifurcations leading to period-4, period-8 and more chaotic behavior devolved to period-2 gait (Figure 4-6).

Another large change in the bifurcation diagram occurred at values above 8.5 N.s.m^{-1} (Figure 4-5). The range of viable stiffness values greatly increased to about 200 N.m^{-1}. The vast majority of ambulatory gaits found were period-1. At damping of 9 N.s.m^{-1}, there was a period-doubling bifurcation at about 125 N.m^{-1} followed by a period-halving bifurcation at approximately 155 N.m^{-1}. At approximately 190 N.m^{-1} a very brief bout of chaotic behavior occurred, which was followed by period-4 behavior until the walker failed. A large increase in stiffness values was observed at 11.0 N.s.m^{-1}. The

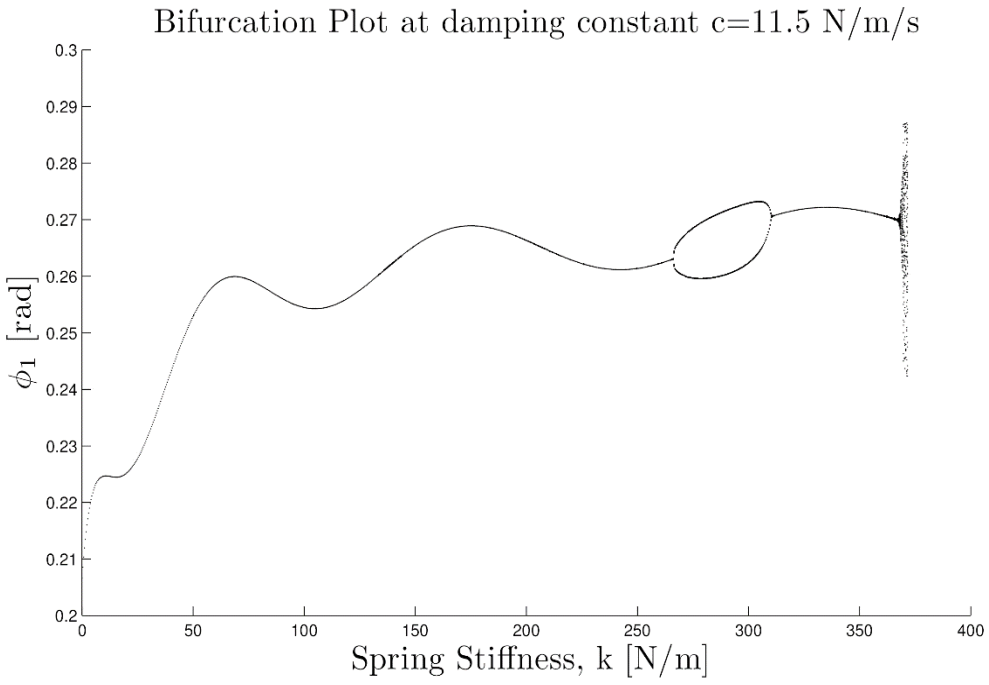

Figure 4-7. Bifurcation diagram at a damping coefficient of 11.5 N.s.m^{-1}. This diagram plots the bifurcation of the stance leg angle, φ_1, against the bifurcation parameter, spring stiffness. The maximum spring stiffness is 370 N.m^{-1}.

bifurcation patterns did not change as drastically in other simulations. The chaotic and subsequent period-4 behavior at 190 $N.m^{-1}$ disappeared. Although, the same behavior appeared at the largest stiffness values (approximately 360-375 $N.m^{-1}$) for 11.0 $N.s.m^{-1}$ damping. There was an additional period-doubling and period-halving bifurcations at approximately 270 $N.m^{-1}$ and 320 $N.m^{-1}$, respectively. The bifurcation plot is very similar at 11.5 $N.s.m^{-1}$ except that the first instance of period-doubling and period-halving disappeared.

Another large increase in stiffness values was observed at 12.0 $N.s.m^{-1}$. Characteristically, the diagram was almost very similar to the bifurcation plot at 11.5 $N.s.m^{-1}$ (Figure 4-7). The difference occurred at stiffness values above the highest values for which the walker ambulated at 11.5 $N.s.m^{-1}$. Two more period-doubling bifurcations followed by period-halving bifurcations occurred, which was followed by chaotic behavior, period-4 behavior, then chaotic behavior before failure at approximately 610 $N.m^{-1}$.

In general, as the damping coefficient was increased the range for which stiffness values resulted in ambulatory gait increased. Furthermore, the period-n, n>1, in each bifurcation diagram were devolved into period-1 gait as the damping parameter increased. Bifurcations with slope as the bifurcation parameter were also analyzed. The spring-damper parameters were chosen based on the most stable parameters according to the LDEs and Floquet multipliers. For all damping parameters, excluding damping between 0.5-1.5 $N.s.m^{-1}$, the gait behavior exhibited period-doubling until chaos and failure. At low levels of damping, there were bouts of chaotic and period-3 behavior at

relatively small slopes (relative to the slope range). These will be discussed further in the following sections.

4.2.3 Local Divergence Exponents

The principal local divergence exponents (LDEs) were calculated throughout a gait cycle for every period-1 gait found for the damping values between 0 and 12 $N.s.m^{-1}$. A LDE with a value below zero is considered stable. Table 4-1 contains the most stable principal LDE and slope range values for each grouping of damping parameters discussed in Section 4.2.1 and the corresponding spring-damper parameters.

Table 4-1. Principal LDE values are the mean LDE values over an entire gait cycle. Slope range was the range of slopes for which the PDW could ambulate. The spring-damper parameters were the values for which the Principal LDE and slope range were found. The control walker was such that the spring-mass-damper system did not affect the gait dynamics.

	Control	Oscillating					
c ($N.s.m^{-1}$)	0	0.00	3.00	8.50	10.50	11.50	12.00
k ($N.m^{-1}$)	0	6.0	4.6	60.6	168.4	168.4	168.3
Principal LDE	1.0069	1.0037	0.9891	0.9610	0.9515	0.9467	0.9444
Slope Range (rad)	0.0143	0.0056	0.0105	0.0187	0.0177	0.0174	0.0171

In terms of the local stability of a gait cycle, the PDWs examined were unstable. Although, as the values for the spring-damper parameters increased, local instability decreased. The maximal and principal LDEs were also found for the same spring-damper parameters for a PDW on varying incline. Passive-dynamic walkers with low spring-damper parameter values (< 3.0 $N.s.m^{-1}$), excluding the control walker, were highly unstable (in a general sense) and could not ambulate on a relatively large range of slopes in period-1 gait (compared with the control walker). The slope range, including the

period-n gait cycles, n = 1, 2, 4…, that the CPDW ambulated was from 0.0046 to 0.190 radians. The principal LDE decreased very slightly as the slope increased for both the control PDW (CPDW) and oscillating PDW (OPDW). The maximum LDE increased very slightly for the oscillating PDW and stayed constant for the control PDW as the slope increased. The largest slope range was found for spring-damper values of 55.5 $N.m^{-1}$ and 3.5 $N.s.m^{-1}$. That range was from 0.0002 radians to 0.0196 radians, which was a 34.7% increase compared with the CPDW.

4.2.3 Floquet Multiplier

The Floquet multipliers were calculated by comparing the initial step conditions from step-to-step following a perturbation. The Floquet multipliers are a measurement of orbital stability. If the Floquet multiplier value is less than unity, then the system was considered stable in the sense of orbital stability. The same spring-damper parameters that were used to calculate the LDE values were used to calculate the Floquet multiplier values. Table 4-2 highlights the most stable spring-damper parameters for each group discussed in Section 4.2.1.

Table 4-2. Floquet multipliers are a measurement of step-to-step stability. The slope range was the range of slopes for which the PDW could ambulate. The spring-damper parameters were the values for which the Floquet multipliers and Slope range were found. The control walker was such that the spring-mass-damper system did not affect the gait dynamics.

	Control	Oscillating					
c ($N.s.m^{-1}$)	0	0.00	0.50	3.50	10.00	12.75	12.00
k ($N.m^{-1}$)	0	0.7	0.7	25.8	32.3	35.6	39.1
Floquet Multiplier	0.5883	0.4167	0.4202	0.3545	0.3644	0.3631	0.3651
Slope Range (rad)	0.0143	0.0144	0.0138	0.0155	0.0176	0.0182	0.0189

In terms of the orbital step-to-step stability, the PDWs were stable. Furthermore, all damping coefficient parameters yielded more step-to-step stability than the control walker. The most stable step-to-step spring-damper parameters were 25.8 $N.m^{-1}$ and 3.5 $N.s.m^{-1}$. The Floquet multiplier value corresponding to those spring-damper parameters was 38.1% less than that of the CPDW. The range of slopes for which the OPDWs could ambulate were calculated for the spring-damper parameters that exhibited the greatest orbital stability. The spring-damper parameters of the OPDW with the largest slope ambulation range were 36.3 $N.m^{-1}$ and 4.75 $N.s.m^{-1}$. The slope range corresponding to that value was 0.0029 radians to 0.0240 radians, which was 88.9% larger than the CPDW slope range.

4.2.4 Basin of Attraction

The basin of attraction (BOA) was estimated for the same spring-damper parameters that were used to calculate the Floquet multipliers. The phase space of the BOA plane was the Poincare section of the initial state for each step. The BOA estimated the size and location of said phase space. The area was normalized by the search area of $1x10^{-12}$ $rad^2.s^{-1}$. For damping values greater than 3.5 $N.s.m^{-1}$, the BOA increased as the

Table 4-3. The area of the basin of attraction was normalized to $1x10^{-12}$ $rad^2.s^{-1}$. The table also includes the mean number of steps the PDW took to reach the gait limit cycle. The control walker was such that the spring-mass-damper system did not affect the gait dynamics.

	Control	----------Oscillating----------					
c ($N.s.m^{-1}$)	0	0	0.5	3.5	10	11.75	12
k ($N.m^{-1}$)	0	0.7	0.7	25.8	32.3	37.6	39.1
Normalized Area	21798	28514	30360	22400	44804	51255	50873

damping and stiffness values increased (Table 4-3). The basin of attraction for values lower than 4.0 N.s.m^{-1}, the BOA did not monotonously increase or decrease as the damping stiffness values increased. . The largest BOA occurred at a damping value of 11.75 N.s.m^{-1} and spring stiffness of 37.6 N.m^{-1}. This BOA was 135.1% larger than the CPDW.

4.2.5 Slope Perturbation Range and Step Time Variability

The slope perturbation range (SPR) was the difference between the maximal and minimal isolated perturbations in the slope that the PDWs could handle without failing to ambulate in the following 200 steps. The SPR was calculated for all spring-damper conditions that resulted in period-1 gait at a ramp slope of 0.009 radians. The SPR value

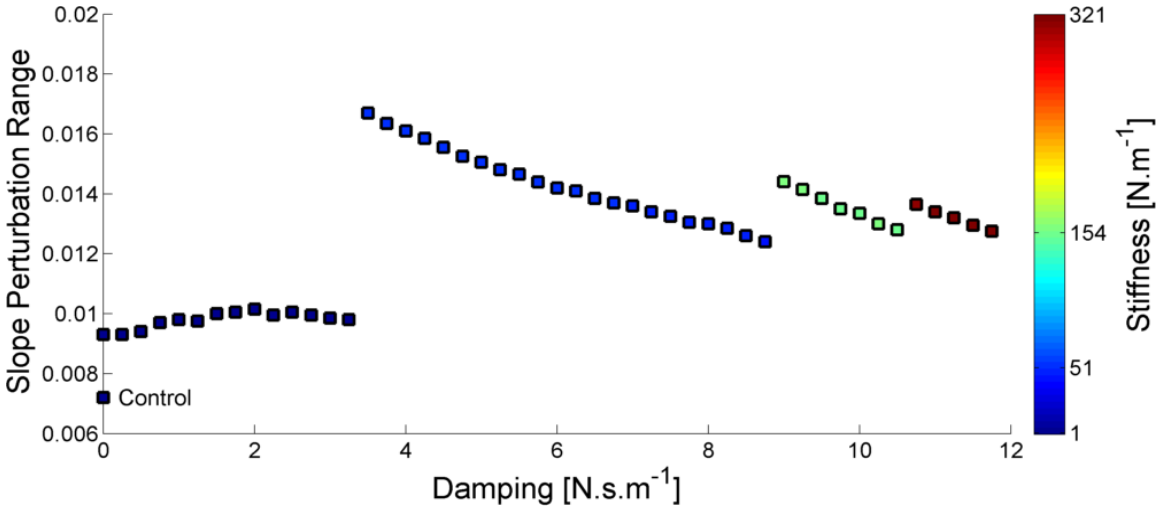

Figure 4-8. A scatter plot of the greatest SPR values for each damping condition. The SPR measured the PDWs robustness to an isolated change in the ramp slope.

for the CPDW was 0.0072 radians. For each damping conditions, the spring stiffness could be tuned such that the SPR value was larger than the SPR value for the CPDW

(Figure 4-8). The SPR value for an OPDW with spring-damper parameters of 53.7 $N.m^{-1}$ and 3.5 $N.s.m^{-1}$ was 0.0167 radians, which was 131.9% greater than the CPDW.

Table 4-4. The step-time variability for the CPDW and the OPDWs with spring-damper conditions that resulted in the lowest STV. The slope was randomly varied by a percentage of the SPR value for the CPDW.

	Control	------Oscillating------		% Difference
c ($N.s.m^{-1}$)	0	5.00	6.75	
k ($N.m^{-1}$)	0	52.6	50.5	
STV at 5% SPR	0.0130	-	0.0087	33.1
STV at 10% SPR	0.0262	-	0.0173	34.0
STV at 15% SPR	0.0397	-	0.0260	34.5
STV at 20% SPR	0.0540	-	0.0347	35.7
STV at 25% SPR	0.0690	0.0432	-	37.4
STV at 30% SPR	0.0851	0.0521	-	38.8
STV at 35% SPR	0.1022	0.0610	-	40.3

The step time variability (STV) was calculated as the standard deviation of the step time of 200 steps on uneven terrain. The slope was randomly varied by a percentage of the SPR value for the CPDW. All spring-damper conditions for which the SPRs were calculated had lower STV. The spring-damper conditions for which the STV was smallest was dependent upon how much the ramp slope varied. At small changes in ramp slope the OPDW with spring-damper conditions of 52.6 $N.m^{-1}$ and 5.0 $N.s.m^{-1}$ had the smallest STV. At larger perturbations, the OPDW with the smallest STV had spring-damper conditions of 50.5 $N.m^{-1}$ and 6.75 $N.s.m^{-1}$, which was 40.3% smaller compared with the CPDW (Table 4-4).

4.3 Summary

The bifurcation diagrams illustrated that the spring-damper parameters could be tuned such that the walker exhibited stable period-1 gait cycles, asymmetric period-n gait cycles (n >1), or chaotic gait cycles. The local stability increased as the values for the spring-damper parameters increased. Orbital stability of the OPDW was up to 38.1% more stable than the CPDW. The range of slopes for which the OPDW could ambulate was up to 88.9% larger than the CPDW. The basin of attraction for the OPDW was up to 135.1% greater than the CPDW. The SPR was up to 131.9% greater than the CPDW. For large variations in the slope from step-to-step, the STV was up to 40.3% less than the CPDW. For all of the aspects of stability that were measured, the spring-damper parameters of the OPDW could be tuned such that the walking gait was more stable.

Chapter 5

Discussion

5.1 Introduction

Passive-dynamic walkers (PDWs) have been utilized to study many aspects of human walking. Stability is very low for a PDW with two degrees of freedom. This thesis has demonstrated that the addition of a spring-mass-damper system to a simple PDW will increase many aspects of stability (e.g., step-to-step stability, or robustness to uneven terrain). Varying the spring-damper parameters can have drastic effects on the stability of a bipedal walker. Although, not all spring-mass-damper systems increase stability to the same degree. Section 5.2 will discuss the implications of the results as they pertain to human walking and PDW walking.

5.2.1 Summary of Findings

It has been illustrated that a PDW with a soft tissue component can increase many aspects of the stability of gait. It has also been illustrated that varying the parameters of the soft tissue substantially affects this stability. Some measures of stability are more sensitive to the soft tissue parameters than others. For example, the spring-damper parameters that resulted in the most stable Floquet multiplier (FM) values did not correspond to the largest basin of attraction (BOA). Furthermore, varying the spring-damper parameters may not have affected the FM values, but had large effects on the BOA area.

In terms of orbital stability, the spring-damper parameters of the OPDW could be tuned such that the walking gait was more stable than the walking gait of the CPDW. Orbital stability was quantified by finding the FM value for the period-1 gait cycles of the OPDW and CPDW. The most stable FM value for the OPDW was 0.3545, which was 39.7% more stable than the CPDW. For a given set of spring-damper parameters, the FM value was dependent upon the slope of the incline. Furthermore, the spring-damper parameters that resulted in the lowest FM values did not correspond to the largest range of ambulatory slopes.

In terms of local stability, all period-1 gait cycles that were tested for the OPDW and CPDW were unstable. However, the local divergence exponent (LDE) values of all period-1 gait cycles for the OPDW indicated that the OPDW was less unstable than the CPDW. As the ambulatory slope increased, the maximum LDE for a gait cycle increased and the principal LDE decreased. The most stable principle LDE value for the OPDW was 0.9444, which was 6.2% more stable than the CPDW.

In terms of the global stability, the spring-damper parameters of the OPDW could be tuned such that the OPDW was more stable than the CPDW. The area of the BOA for the CPDW and OPDW were relatively small. The largest BOA for the OPDW was 135.1% greater than that of the CPDW.

The slope perturbation range (SPR) and step time variability (STV) were measures of robustness to environmental perturbations. For each damping condition the spring stiffness could be tuned such that the SPR value was greater for the OPDW compared with that of the CPDW. The largest SPR value was 131.9% greater for the OPDW than that of the CPDW. The STV was dependent upon how much the slope was

varied from step-to-step. For relatively large slope variations, the STV for the OPDW was up to 40.3% less than that of the CPDW.

5.2.2 Interpretation of Findings

Stability, in terms of human walking, is mostly associated with the ability to walk without falling. However, it is still unclear what measures of stability are the best predictors of falling. Furthermore, the mode at which the perturbation is applied (e.g., an external force or a change in the terrain) may change the stability measurement that is best at predicting a fall. To date, there is no literature that reports on the effects of spring-damper parameters of the soft tissue component in a PDW on multiple aspects of stability and spatiotemporal variability.

Su and Dingwell (2007) found that the orbital stability of a compass walker was not correlated with the amplitude of a perturbation, and that FM values are poor predictors of PDW failure. It may be that FMs are not well suited at determining a PDW's response to external perturbations, but rather it assesses a PDW's sensitivity to variations in its internal structure. In this study, the amplitude of the applied perturbations to the PDW's state were held constant, but the spring-damper parameters were varied. Varying the spring-damper parameters substantially changed the FM values. Granata and Lockhart (2008) reported that the orbital stability, as measured by FMs, of a fall-prone geriatric population was significantly lower compared with that of a younger population ($p < 0.05$). It is well established that elderly populations have a higher body fat percentage (Fukagawa et al., 1990; Micozzi and Harris, 1990). Muscle

and tendon tissues, which are dense in collagen and other elastic structures, have different mechanical properties than adipose tissue. These findings suggest that altering the mechanical properties of soft tissue affects the orbital stability of bipedal walking. It may be that lower orbital stability in elderly populations is due, in part, to different body mass composition.

It is not uncommon for human gait to be orbitally stable while simultaneously exhibiting local instability (Dingwell and Kang, 2006; Su and Dingwell, 2007; Schablowski and Gerner, 2006). Local divergence exponents calculate the divergence (or convergence) of small perturbations within a relatively short time span (<1% of step time). The entire gait cycle, excluding the switch between stance leg and swing leg, of the CPDW and OPDW was locally unstable. This indicates that the switching condition between the stance and swing legs plays a crucial role in locally stabilizing a PDW simulation that does not include a model of the double-support phase. The LDE values for these findings indicate that the compass walker is more unstable compared to that of humans (Buzzi et al., 2003). Corrective measures that humans use to stabilize gait are affected by many components of the human body (e.g., proprioceptors, neuromuscular system, and musculotendon dynamics). However, the evidence suggests that healthy human walking is subject to instability that is due, in part, to the primal dynamics of bipedal gait.

Some research has suggested that STV is significantly different amongst age groups (Beauchet et al., 2009; Yogev-Seligmann et al., 2010) and may reflect the risk of falling (Roos and Dingwell, 2010; Su and Dingwell, 2007). These findings found that increased terrain variability led to increased STV variability in PDWs. However, the

OPDW was affected by the terrain variability to a lesser extent compared with the CPDW. Beauchet et al. (2009) reported that older populations walk slower to maintain low STV. The OPDWs with the lowest STV had a higher walking velocity. It may be that STV in human subjects is in part due to the intrinsic properties of the human body.

The BOA is a long-term measurement of step-to-step stability. The stability of the OPDW in terms of the BOA had the largest relative increase compared with the CPDW. Furthermore, the BOA varied by a relatively large amount for period-1 gait cycles compared to the other aspects of stability. This indicates that soft tissue may play a relatively large role in global stability of human walking.

A stable gait cycle in a physical PDW is heavily dependent upon the initial conditions that the handler procures. A PDW with a large BOA would be the easiest to produce stable walking gait. This research suggests that a PDW with a mass oscillator about the pelvis can have a greater BOA and make the PDW less sensitive to the initial state that the handler procures for the walker. Adding a spring-mass-damper system would be relatively simple compared to actuating a PDW. The spring-mass-damper system is completely passive and therefore a highly efficient method of stabilizing a robotic walker.

Similar to the BOA, the maximum slope perturbation (SPR) and STV are more applicable tests of stability than FMs because the ground for which the PDW will ambulate may not be uniformly flat. Maximum slope perturbation and STV directly measured the robustness of the PDWs to changes in the environment. It has been shown that the stability of PDWs on mildly rough terrain (0.1% of leg length variability) is very low (Afshar and Ren, 2012). Various methods that require joint actuation have been

implemented in order to stabilize compass PDWs on rough terrain (e.g., Iida and Tedrake, 2010; Manchester et al., 2011; Park, 2012). These control systems can be very complex and impossible to implement in a physical PDW. Change in floor height is an inevitable circumstance for humans and robotic walkers. Therefore, it is crucial that robotic walkers can maintain stability on rough terrain.

The OPDWs, which could handle a range of floor height perturbations up to 131.9% greater than the CPDW, exhibited greater robustness to terrain variability. This indicated that passive robustness may be obtainable in PDW systems. The benefit to using a passive system is two-fold: the method of control is relatively simple to simulate, and the controller easier to implement in a physical system compared to walkers that are not based on PDWs (Collins et al., 2005). To include a complex controller in a physical system means that the PDW must be wired to a computer external to the PDW or the PDW must carry a computer and battery. Connecting a PDW to an external computer means that the researcher must place the PDW on a boom to compensate for the instability caused by wires. Connecting a PDW to a battery and computer makes the problem of addressing stability and mass distribution more difficult.

Short-term robustness is a better measurement for a PDWs ability to overcome a single obstacle (e.g., SPR). However, the STV gives a better prediction of how an OPDW would react to real-world variability in terrain for long-term tasks. The change in floor height could be described as environmental noise. The STV variability has been used in PDWs to study the effects of controller noise on PDW ambulation (Roos and Dingwell, 2010). In a real setting, there will be a level of random and systematic noise due to the environment and controller system. It may be that an oscillating mass may

increase the PDWs robustness to noise and increase the long-term stability in an environment with varying floor height, this warrants investigation. A further elaboration on the non-linear dynamics of the PDWs is provided in Appendix A.

5.3 Study Limitations

Limitations to the study are associated with the modeling of the bipedal walker. The first limitation is the nature of the foot-ground contact event. The foot is modeled as point mass connected to the ground via a hinge joint. This could be more realistic if the contact element was elastic and the foot was rounded. Furthermore, this contact would have enabled a more sophisticated model that included a double-support phase. The soft tissue component would affect the gait dynamics of the single-support phase differently than that of the double-support phase. The contact dynamics between the PDW and the ground would heavily influence the subsequent dynamics of a soft tissue component. Larger contact forces would cause larger oscillations that have a larger amplitude and higher frequency modes. A nonlinear spring-damper system would need to be implemented to account for this.

Due to the low stiffness and damping values that were used to measure stability, the acceleration of the soft tissue in the vertical direction did not include a gravitational acceleration component. If the effects of gravity were included in the soft tissue component of the model, then the weight of the soft tissue would extend the spring such that the mass was well below the ground. A *post-hoc* analysis revealed that including gravitational acceleration to the soft tissue component of a PDW does have an effect on

the orbital and local stability. The Floquet multiplier value of an OPDW (without gravity acting on the soft tissue component) with spring-damper parameters of 25.8 $N.m^{-1}$ and 11.5 $N.s.m^{-1}$ was 0.5938. The Floquet multiplier value of an OPDW with the same spring-damper parameters, but with gravity acting on the soft tissue component, was 0.5520. This indicates that the OPDW with gravity acting on the soft tissue component was more orbitally stable compared to the alternative. However, an OPDW with spring-damper parameters of 25.8 $N.m^{-1}$ and 3.5 $N.s.m^{-1}$ was oppositely affected. The Floquet multiplier value was less in magnitude for the OPDW without gravity acting on the soft tissue component compared with an OPDW with gravity acting on the soft tissue component. More research is needed to investigate the effects of a soft tissue component under the influence of gravity on the gait stability of PDWs.

5.4 Future Research Direction

The next step in analyzing the effects of soft tissue on walking dynamics in humans is to make the PDW model more realistic. The following is a list of the components that may be added in future model designs: rounded feet, elastic foot-ground contact, legs with soft tissue mass, knee and ankle joints, neuromuscular control of the joints, or a double-support phase. Careful analysis can reveal how the stability of gait dynamics is affected by adding these components.

Another future study could extend the two-dimensional PDW into three dimensions to examine the effects of soft-tissue oscillation on three-dimensional gait dynamics. Modeling three-dimensional PDWs with rounded feet is a method for

eliminating foot scuffing without the inclusion of knees. This would enable the walker to remain relatively simple and simulate PDW gait dynamics in a more realistic setting.

An exciting study would be to apply this work to a physical PDW. Soft tissue vibration can be designed using many different materials. For example, a physical PDW with a hollow pelvis can accommodate a silicon mold that vibrates during PDW ambulation. Furthermore, a simple control system with an actuator can be added to enable ambulation on a zero-degree incline. A robotic walker that can walk for an extended period of time could provide enough kinematic and kinetic data to measure many aspects of walking gait stability.

5.5 Thesis Conclusion

This study presented evidence that soft tissue may contribute in many aspects of human walking stability. A passive-dynamic walker with a soft tissue component was more stable than the passive-dynamic walker without a soft tissue component as assessed by Floquet multipliers, local divergence exponents, the basin of attraction, slope perturbation range, and the step time variability. This indicated that mass vibration may be an effective method to passively stabilize a bipedal walker. This study provided insight into the gait dynamics of passive-dynamic walkers with a soft tissue component and has built a framework for future studies that address the effects of soft tissue vibration on human and robotic walking dynamics.

References

Afshar, P. N., & Ren, L. (2012). Dynamic Stability of Passive Bipedal Walking on Rough Terrain: A Preliminary Simulation Study. *JOURNAL OF BIONIC ENGINEERING*, *9*(4), 423 – 433.

Beauchet, O., Allali, G., Annweiler, C., Bridenbaugh, S., Assal, F., Kressig, R. W., & Herrmann, F. R. (2009). Gait Variability among Healthy Adults: Low and High Stride-to-Stride Variability Are Both a Reflection of Gait Stability. *Gerontology*, *55*(6), 702–706.

Buzzi, U. H., Stergiou, N., Kurz, M. J., Hageman, P. A., & Heidel, J. (2003). Nonlinear dynamics indicates aging affects variability during gait. *Clinical Biomechanics*, *18*(5), 435–443.

Cavagna, G. A., Heglund, N. C., & Taylor, C. R. (1977). Mechanical work in terrestrial locomotion: two basic mechanisms for minimizing energy expenditure. *The American Journal of Physiology*, *233*(5), R243–261.

Cavagna, G. A., Thys, H., & Zamboni, A. (1976). The sources of external work in level walking and running. *The Journal of Physiology*, *262*(3), 639–657.

Collins, S. H., Wisse, M., & Ruina, A. (2001). A Three-Dimensional Passive-Dynamic Walking Robot with Two Legs and Knees. *The International Journal of Robotics Research*, *20*(7), 607 – 615.

Collins, S., Ruina, A., Tedrake, R., & Wisse, M. (2005). Efficient Bipedal Robots Based on Passive-Dynamic Walkers. *Science*, *307*(5712), 1082 – 1085.

Cvitanović, P., Gunaratne, G. H., & Procaccia, I. (1988). Topological and metric properties of H'enon-type strange attractors. *Physical Review A*, *38*(3), 1503–1520.

Dean, J. C., & Kuo, A. D. (2009). Elastic coupling of limb joints enables faster bipedal walking. *Journal of the Royal Society Interface*, *6*(35), 561–573.

Dingwell, J. B., & Kang, H. G. (2006). Differences Between Local and Orbital Dynamic Stability During Human Walking. *Journal of Biomechanical Engineering*, *129*(4), 586–593.

Fukagawa, N. K., Bandini, L. G., & Young, J. B. (1990). Effect of age on body composition and resting metabolic rate. *American Journal of Physiology - Endocrinology and Metabolism*, *259*(2), E233–E238.

Garcia, M., Chatterjee, A., Ruina, A., & Coleman, M. (1998). The Simplest Walking Model: Stability, Complexity, and Scaling. *Journal of Biomechanical Engineering*, *120*(2), 281–288.

Gates, D. H., & Dingwell, J. B. (2007). Peripheral neuropathy does not alter the fractal dynamics of stride intervals of gait. *Journal of Applied Physiology*, *102*(3), 965–971.

Gates, D. H., Su, J. L., & Dingwell, J. B. (2007). Possible biomechanical origins of the long-range correlations in stride intervals of walking. *Physica a-Statistical Mechanics and Its Applications*, *380*, 259–270.

Gear, C. W. (1971). *Numerical initial value problems in ordinary differential equations*. Prentice-Hall.

Granata, K. P., & Lockhart, T. E. (2008). Dynamic stability differences in fall-prone and healthy adults. *Journal of Electromyography and Kinesiology*, *18*(2), 172–178.

Gregg, R., Dhaher, Y., Degani, A., & Lynch, K. (2012). On the Mechanics of Functional Asymmetry in Bipedal Walking.

Hilborn, R. C. (2000). *Chaos and nonlinear dynamics: an introduction for scientists and engineers* (2nd ed.). Oxford: Oxford University Press.

Hobbelen, D. G. E., & Wisse, M. (2007). A Disturbance Rejection Measure for Limit Cycle Walkers: The Gait Sensitivity Norm. *IEEE Transactions on Robotics*, *23*(6), 1213–1224.

Hu, B., & Zhao, M. (2012). The optimization of spring stiffness for passive dynamic walker. In *2012 IEEE/RSJ International Conference on Intelligent Robots and Systems (IROS)* (pp. 1943–1949).

Iida, F., & Tedrake, R. (2010). Minimalistic control of biped walking in rough terrain. *Autonomous Robots*, *28*(3), 355–368.

Li, Q., & Yang, X.-S. (2012). New walking dynamics in the simplest passive bipedal walking model. *Applied Mathematical Modelling*, *36*(11), 5262–5271.

Manchester, I. R., Mettin, U., Iida, F., & Tedrake, R. (2011). Stable dynamic walking over uneven terrain. *The International Journal of Robotics Research*, *30*(3), 265–279.

McGeer, T. (1990). Passive Dynamic Walking. *The International Journal of Robotics Research*, *9*(2), 62 – 82.

McGeer, T., & Palmer, L. H. (1989). Wobbling, Toppling, and Forces of Contact. *American Journal of Physics*, *57*(12), 1089 – 1098.

McMahon, T. A. (1984). Mechanics of Locomotion. *The International Journal of Robotics Research*, *3*(2), 4–28.

Micozzi, M. S., & Harris, T. M. (1990). Age variations in the relation of body mass indices to estimates of body fat and muscle mass. *American Journal of Physical Anthropology*, *81*(3), 375–379.

Milner, M., & Quanbury, A. O. (1970). Facets of Control in Human Walking. *Nature*, *227*(5259), 734–735.

Pain, M. T., & Challis, J. H. (2002). Soft Tissue Motion During Impacts: Their Potential Contributions to Energy Dissipation. *Journal of Applied Biomechanics*, *18*(3).

Pain, M. T. G., & Challis, J. H. (2006). The influence of soft tissue movement on ground reaction forces, joint torques and joint reaction forces in drop landings. *Journal of Biomechanics*, *39*(1), 119–124.

Park, H. W. (2012). *Control of a Bipedal Robot Walker on Rough Terrain* (Ph.D.). University of Michigan, United States -- Michigan.

Piazza, S. J., & Delp, S. L. (1996). The influence of muscles on knee flexion during the swing phase of gait. *Journal of Biomechanics*, *29*(6), 723–733.

Roos, P. E., & Dingwell, J. B. (2010). Influence of simulated neuromuscular noise on movement variability and fall risk in a 3D dynamic walking model. *Journal of Biomechanics*, *43*(15), 2929–2935.

Rosenblatt, N. J., & Grabiner, M. D. (2010). Measures of frontal plane stability during treadmill and overground walking. *Gait & Posture*, *31*(3), 380–384.

Schablowski, M., & Gerner, H. J. (2006). Comparison of Two Measures of Dynamic Stability During Treadmill Walking. In M. Diehl & K. Mombaur (Eds.), *Fast*

Motions in Biomechanics and Robotics (pp. 345–360). Springer Berlin Heidelberg.

Schwab, A. L., & Wisse, M. (2001). Basin of Attraction of the Simplest Walking Model. *Proceedings of Design Engineering Technical Conferences and Computers and Information in Engineering Conference*.

Su, J. L.-S., & Dingwell, J. B. (2007). Dynamic Stability of Passive Dynamic Walking on an Irregular Surface. *Journal of Biomechanical Engineering*, *129*(6), 802–810.

Usherwood, J., Channon, A., Myatt, J., Rankin, J., & Hubel, T. (2012). The Human Foot and Heel-Sole-Toe Walking Strategy: A Mechanism Enabling an Inverted Pendular Gait with Low Isometric Muscle Force. *Journal of the Royal Society Interface*, *9*(75), 2396 – 2402.

Wisse, M., Schwab, A. L., & van der Helm, F. C. T. (2004). Passive Dynamic Walking Model with Upper Body. *Robotica*, *22*(6), 681 – 688.

Yamasaki, M., Sasaki, T., Tsuzuki, S., & Torii, M. (1984). Stereotyped pattern of lower limb movement during level and grade walking on treadmill. *The Annals of Physiological Anthropology*, *3*(4), 291–296.

Yogev-Seligmann, G., Rotem-Galili, Y., Mirelman, A., Dickstein, R., Giladi, N., & Hausdorff, J. M. (2010). How Does Explicit Prioritization Alter Walking During Dual-Task Performance? Effects of Age and Sex on Gait Speed and Variability. *Physical Therapy*, *90*(2), 177–186.

Zatsiorky, V. M., Werner, S. L., & Kaimin, M. A. (1994). Basic kinematics of walking. Step length and step frequency. A review. *The Journal of Sports Medicine and Physical Fitness*, *34*(2), 109–134.

Appendix A

Additional Analysis of Passive-Dynamic Walking Gait Dynamics

Bifurcation Diagrams and Floquet Multipliers

Floquet multipliers are a measure of orbital stability. A Floquet multiplier value that crosses unity (FM value ≥1) is indicative of a limit cycle that becomes unstable. In a bifurcation diagram, this can be visualized by a period-1 to period-2 bifurcation. That is, the FM value crosses unity at the bifurcation. The spring-damper parameters of an

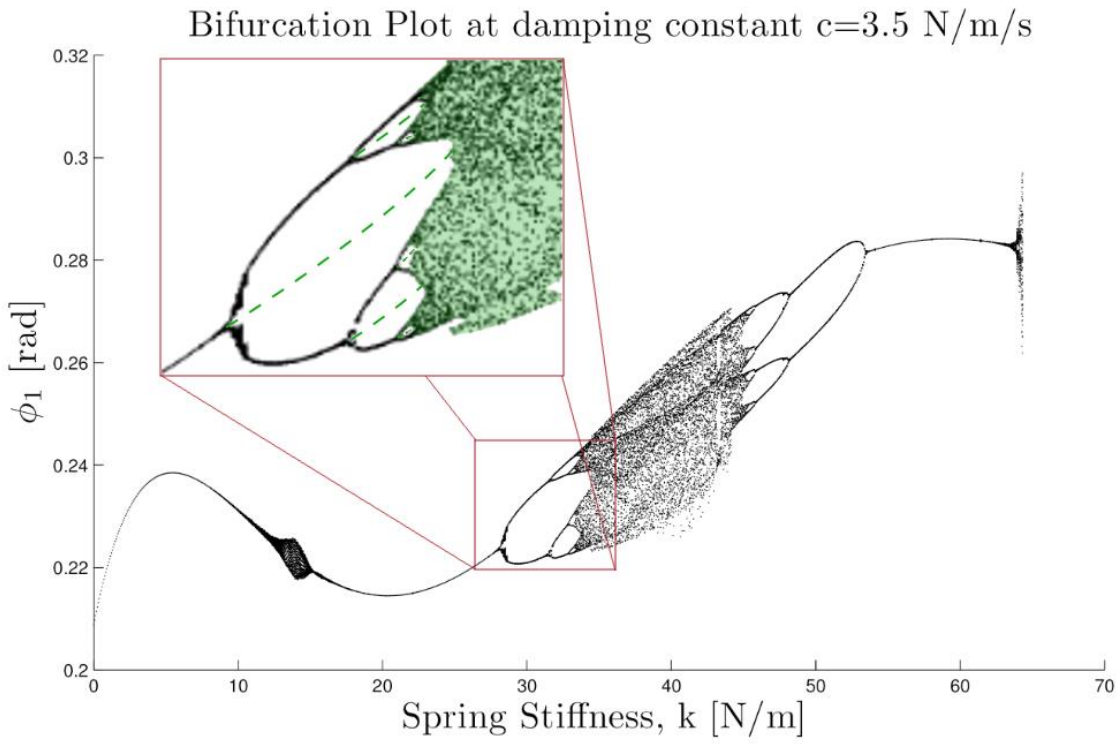

Figure A-1. A bifurcation diagram with unstable equilibria and chaos highlighted in green. The unstable equilibria are marked by a dashed green line. Chaos is highlighted by a green area.

oscillating passive-dynamic walker (OPDW) could be tuned such that the gait was asymmetric. However, period-2 gait is stable in the general sense that the PDWs will still ambulate indefinitely. The same is true for higher order periods and chaotic gait.

For most damping conditions, a series of period-doubling bifurcations were followed by a series of period-halving bifurcations until the OPDW returned to a period-1 gait cycle as stiffness increased. The period-doubling bifurcations that lead to chaos are pitchfork bifurcations (Figure A-1); which means that the stable equilibria bifurcate and an unstable equilibrium appear at each bifurcation. The unstable equilibria are repelling the fixed-point limit cycle away from the unstable equilibria. The stable equilibria attract the fixed-point limit cycle. The system enters chaos whenever all equilibria become unstable.

The mechanical energy (ME) of the initial state of each gait cycle (i.e., the fixed points) will oscillate around their corresponding unstable equilibria. That is, during a period-2 limit cycle, the ME of the fixed point of the first gait cycle will be higher than the ME of the unstable fixed point equilibrium. Subsequently, the ME of the second fixed point of the period-2 limit cycle will be lower than the ME of the unstable fixed point equilibrium. This oscillation becomes more complex as the period-n limit cycle order becomes larger (Figure A-2). For example, the first gait cycle of a period-8 gait cycle will be one with the largest positive ME difference from the unstable fixed point equilibrium. The following gait cycle will be the largest negative ME difference from the unstable fixed point equilibrium. The third fixed point will be the smallest positive mechanical energy difference from the unstable fixed point. The fourth point will be the smallest negative ME difference from the unstable fixed point. The ME oscillation continues with the second-most largest positive ME difference from the unstable fixed point. The ME of the gait cycles for the period-8 limit cycle oscillate around the original unstable fixed point (i.e., the unstable limit cycle that originates during the period-1 to period-2 pitchfork bifurcation).

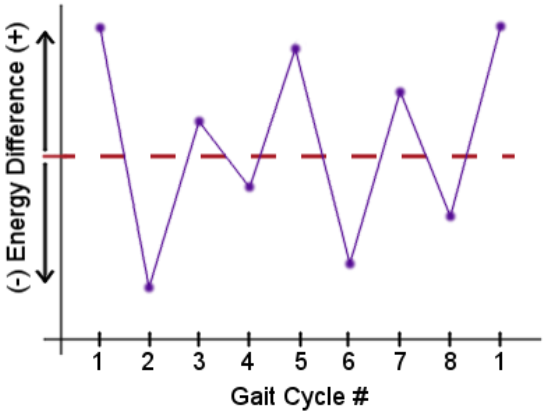

Figure A-2. The energy difference between the unstable equilibrium that resulted from the first bifurcation of a series of bifurcations and the stable equilibria of a period-8 limit cycle. The red dashed line is the mechanical energy of the fixed point of an unstable period-1 limit cycle. The purple dots are the mechanical energy of each fixed point of a period-8 gait cycle.

The most stable period-1 gait cycles in terms of FMs occurred before the first pitchfork bifurcation for each damping condition. The period-1 gait cycles that occurred after the period-halving series are ambulating at a faster velocity, and, consequently, have more kinetic energy. These FM values for these period-1 gait cycles are higher than that of the control walker. Furthermore, the lowest walking velocity for every damping condition occurred at a spring stiffness of 0 $N.m^{-1}$. These values also had a larger FM value. Before the first period-doubling bifurcation, the eigenvalues of the Jacobian in Equation (10) are equal; at which the normalized FM value is smallest. As the stiffness was increased, the eigenvalues of said Jacobian diverged and the eigenvalue associated with the stance leg angular velocity, $\dot{\varphi}_1$, crossed unity while the eigenvalue associated with stance leg angle, φ_1, remained less than unity. This indicates that instability at these values of damping and stiffness are a result of angular velocity instability.

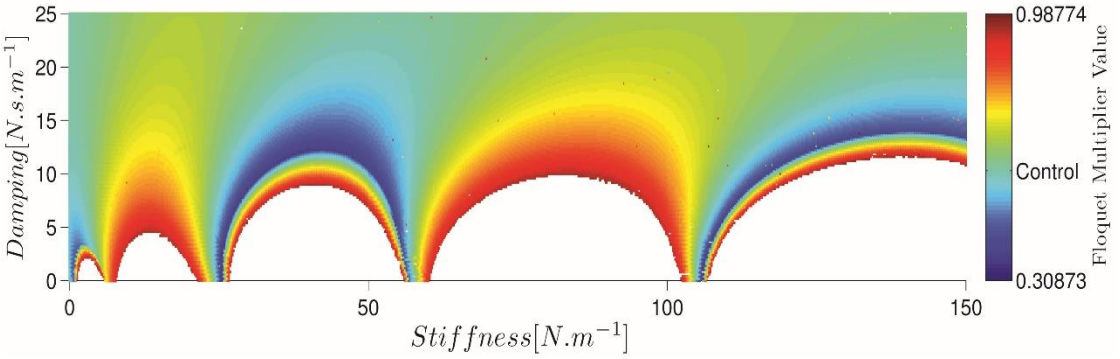

Figure A-4. A spectrum of FM values for period-1 stable limit cycles with varying spring-damper parameters. White space indicates that no period-1 limit cycles were found.

A *post hoc* analysis of FMs was performed in order to find stable period-1 gait cycles beyond spring stiffness values previously reported in Chapter 4. A pattern of period-1 limit cycle stability according to the FM values can be visualized in Figure A-4. Each arch is bordered by a red band (where the FM value is approaching unity). Every

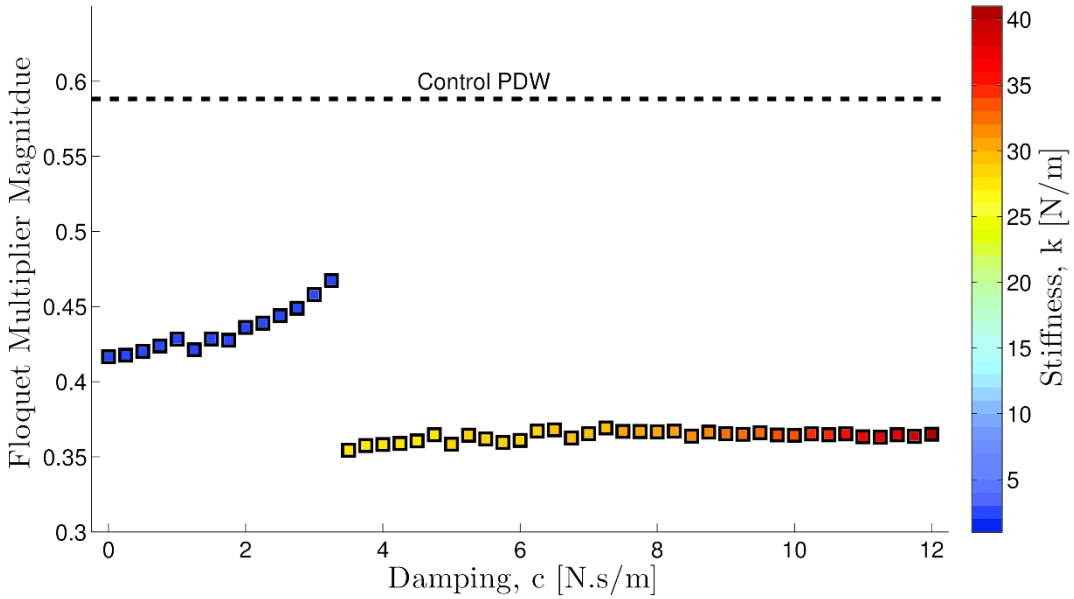

Figure A-3. The FM values that were calculated below damping values of 3.5 $N.s.m^{-1}$ occurred in the first stable band located in the bottom-left corner of Figure A-4 between stiffness values of 0 $N.m^{-1}$ and 1 $N.m^{-1}$. The FM values that were calculated for damping values greater than and equal to 3.5 $N.s.m^{-1}$ occurred in blue spectrum of Figure A-4 between stiffness values of 25 $N.m^{-1}$ and 40 $N.m^{-1}$.

second arch is surrounded by a blue band, which corresponds to high stability relative to the CPDW. The arches that are surrounded by the blue band correspond to period-1 to period-2 bifurcations due to instability of the stance leg angular velocity. The *post hoc* analysis revealed that the spring-damper values that corresponded to the highest stability according to FMs occurred between damping values of 3.5 $N.s.m^{-1}$ and 15 $N.s.m^{-1}$ and between stiffness values of 25 $N.m^{-1}$ and 55 $N.m^{-1}$ (Figure A-3).

The FM values that cross unity at spring stiffness values after the series of period-halving are not a result of unstable stance leg velocity. The eigenvalue of the Jacobian in Equation (10) that is linked to the stance leg angle, crosses unity while the other eigenvalue that corresponded to the stance leg angular velocity remains below unity. That is, the walker loses stability due to the instability of the angular position. The arches in Figure A-4 that are not surrounded by a blue band are indicative of when the angular position becomes unstable. These arches correspond to bifurcations from a period-1 limit cycle to a period-2 limit cycle or period-1 limit cycle to a chaotic limit cycle. If the spring-damper parameters are incremented such that they are approaching the center of an arch, the routes to chaos are very short and dramatic.

The eigenvalues for the Jacobian in Equation (10) for all of the period-n, $n>1$, limit cycles were indicative of *saddle cycles*. That is, one eigenvalue was less than unity while the other eigenvalue was greater than unity. Furthermore, the eigenvalues have a component in the real and complex planes, which indicates that the limit cycles are *spiral saddle cycles*. A spiral saddle cycle is one in which a trajectory that is converging to the period-2 limit cycle approaches the limit cycle while simultaneously spiraling around the limit cycle. For example, imagine a tornado that is twisting touches the ground at a

single point. The stable limit cycle could be seen as the axis about which the tornado is swirling around. As you descend into the tornado, the width of the rotating air decreases until it reaches zero (at the ground). Imagine you are a piece of dust that is sitting perfectly on the eye of tornado (the axis of rotation). Assuming that the air is not moving the dust, it would drop in free fall along the eye of the tornado. However, if that piece of dust has its path of descent disturbed while it was descending, it would start twirling around the eye of the tornado as it descended. Furthermore, as the piece of dust descended, it would get closer to the eye of the tornado because the width of rotating air is shrinking. The trajectories of the passive walker behave in a similar fashion. As they converge to the stable limit cycle, they also spiral around it.

A change in the spring-damper parameters forces a change in the walking velocity by means of changing the required initial conditions for stable locomotion. At larger walking velocities, the damping component of the spring-damper system will have a larger effect on the amount of energy that is being dissipated. Therefore, the higher spring stiffness values increase the walking speed of stable locomotion, which subsequently affects the amount of energy dissipation. The spring-damper parameters and walking velocity will subtly interact and affect the FM values.

Chaotic Gait Cycles and Strange Attractors

Chaotic gait cycles are such that two initial conditions that are arbitrarily close result in trajectories that diverge exponentially every step. In the case of the PDWs, these types of gait cycles are caused by a *strange attractor*. A strange attractor is a general

term for a limit cycle attractor that is characterized by an unusual shape. A strange attractor is typically a result of a series of period-doubling bifurcations that become unstable. However, a strange attractor can appear due to the overlap of an unstable gait with a stable period-1 gait cycle. The trajectories of an attracting limit cycles overlap very briefly and the gait cycle will converge to the strongest attracting limit cycle (Li and Yang, 2012). These attractors can be found if the numerical analysis is at a resolution high enough to approach the intersection (which is extremely brief) of the separate attracting limit cycles. Furthermore, the strange attractor must be stronger than the period-1 limit cycle attractor to pull the stable period-1 limit cycle to the unstable chaotic cycle. Figure A-5 illustrates an example of a strange attractor intersecting the same state space as a period-1 limit cycle attractor. However, as the slope continued to decrease, the period-1 limit cycle attractor became stronger and pulled the gait cycle back to the period-1 limit cycle.

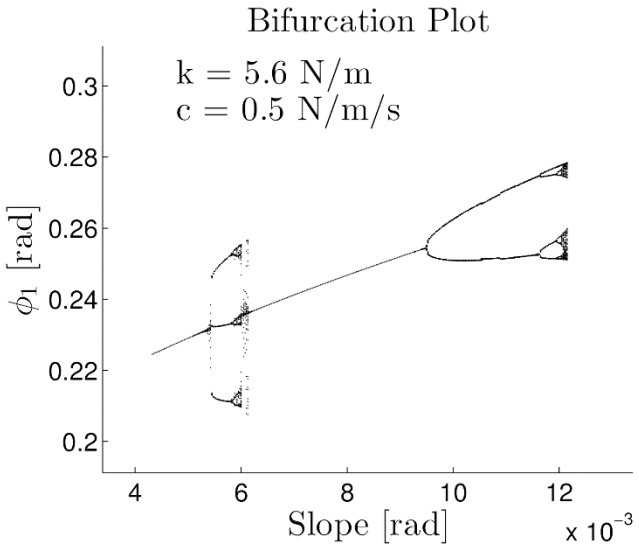

Figure A-5. Bifurcation plot of a the initial stance angle, ϕ_1, and the ramp slope as the bifurcation parameter. The OPDW has spring-damper parameters of 5.6 N.m^{-1} and 0.5 N.s.m^{-1}.

Finding and analyzing the strange attractor gait cycles could be a thesis on its own. The existence of strange attractors and how they influence bipedal walkers is still largely uncharted territory. Some strange attractors are much stronger than others. The

OPDWs that have a larger set of spring-damper parameters for which the motion is chaotic indicates that the strange attractors are stronger. However, the expense of having strong strange attractors in the case of the PDW is that the gait cycles enters chaos at smaller slope values (Figure A-6).

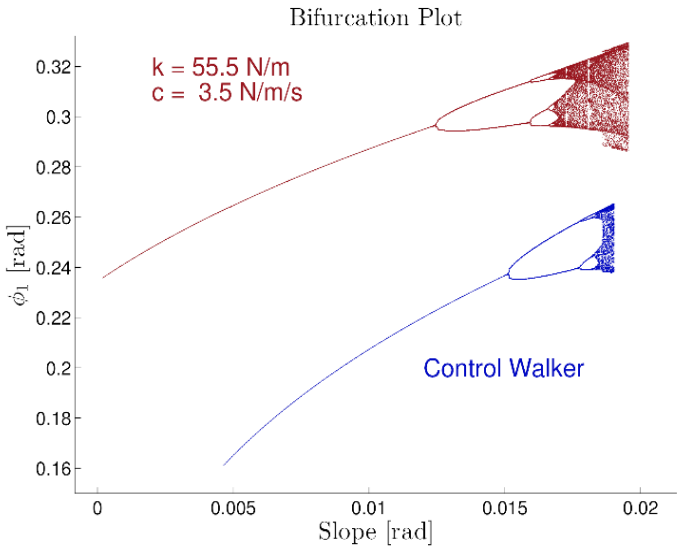

Figure A-6. Bifurcation diagram of the initial stance angle, ϕ_1, with respect to the slope. An OPDW with spring-damper parameters of 55.5 N.m^{-1} and 3.5 N.s.m^{-1} is plotted next to the CPDW.

The strange attractor that is stronger has a larger basin of attraction (BOA) than a strange attractor that is weaker. The border of the BOA is tangent to the border of the strange attractor (Cvitanović et al., 1988), thus it may be beneficial to have a strong strange attractor. Further research needs to be done in order to determine if the BOA of a strong strange attractor are potentially larger than the strong attractors of a period-1 limit cycle and the conditions for which this might occur.

The Basin of Attraction

The BOA may be both one of the most simple and most insightful measurements of stability. Different initial conditions for a gait cycle are simulated to test whether the walker will fail or converge to the original limit cycle. It is important to distinguish

between returning to the original limit cycle or another attracting limit cycle; with the right initial conditions, the PDW can converge to a completely different gait cycle. This is an effective method for finding other attractors (e.g., period-n, n ≥ 1 and strange attractors). The area of the BOA monotonously increases or decreases as the bifurcation parameter is incremented (Schwab and Wisse, 2001). Finding breaks in the monotonous change in the area of BOA is a sign that another attractor is nearby.

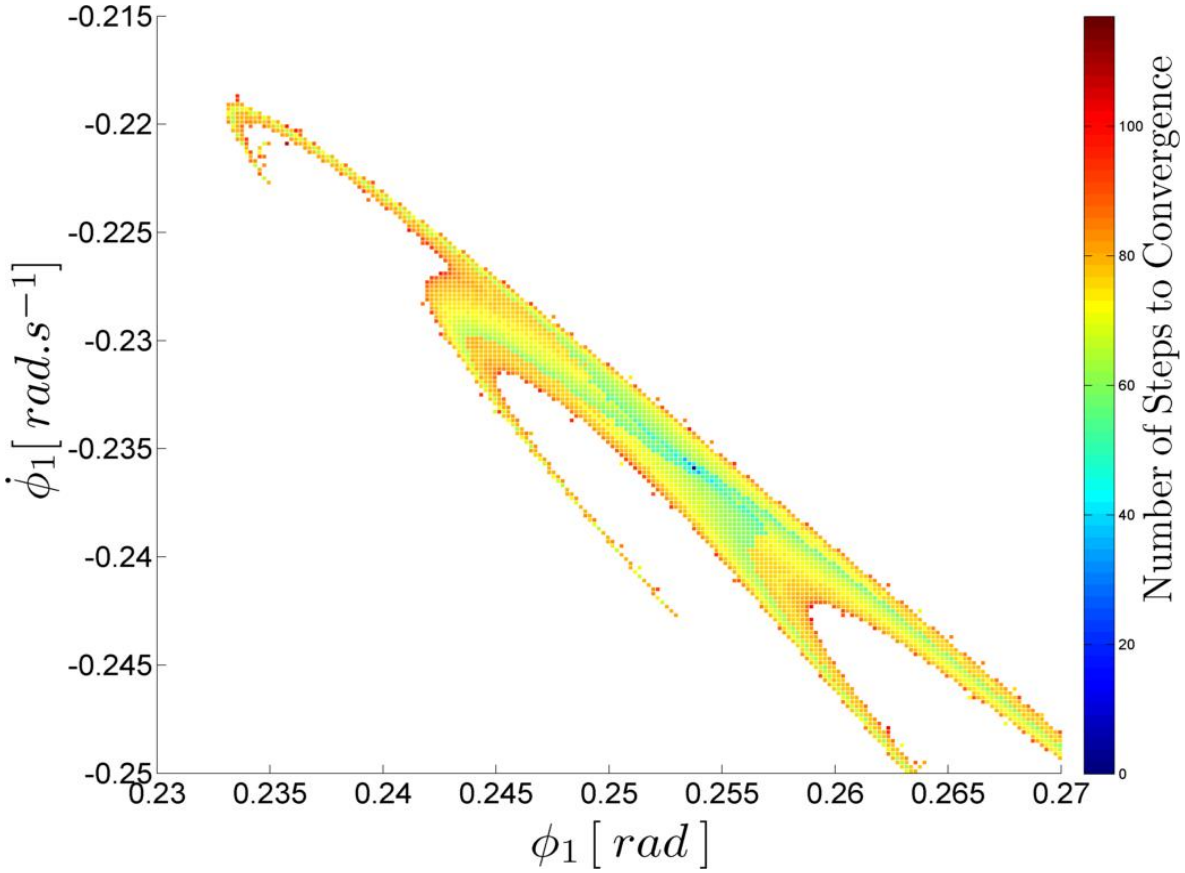

Figure A-7. The basin of attraction for an OPDW with spring-damper parameters of 94.9 $N.m^{-1}$ and 9.25 $N.s.m^{-1}$. This basin of attraction is fractal. The area may have been underestimated if a portion of the basin of attraction was not directly adjacent to the one illustrated here.

In a linear system, the initial distance from the equilibrium point is directly proportional to how much time (or, in this case, steps) it takes to reach the equilibrium. However, this is not the case for the CPDW and OPDW because the systems are nonlinear. Furthermore, the BOA for the OPDW are fractal (Figure A-7). That is, the border of the BOA is not continuous. The search method that was implemented in this analysis may have underestimated the area of the BOA for the OPDW. Fractal basins of attraction do not have to be adjacent, however this search method assumed that the BOA was closed. The results of Schwab and Wisse (2001) indicated that the BOA area of the CPDW was not underestimated.

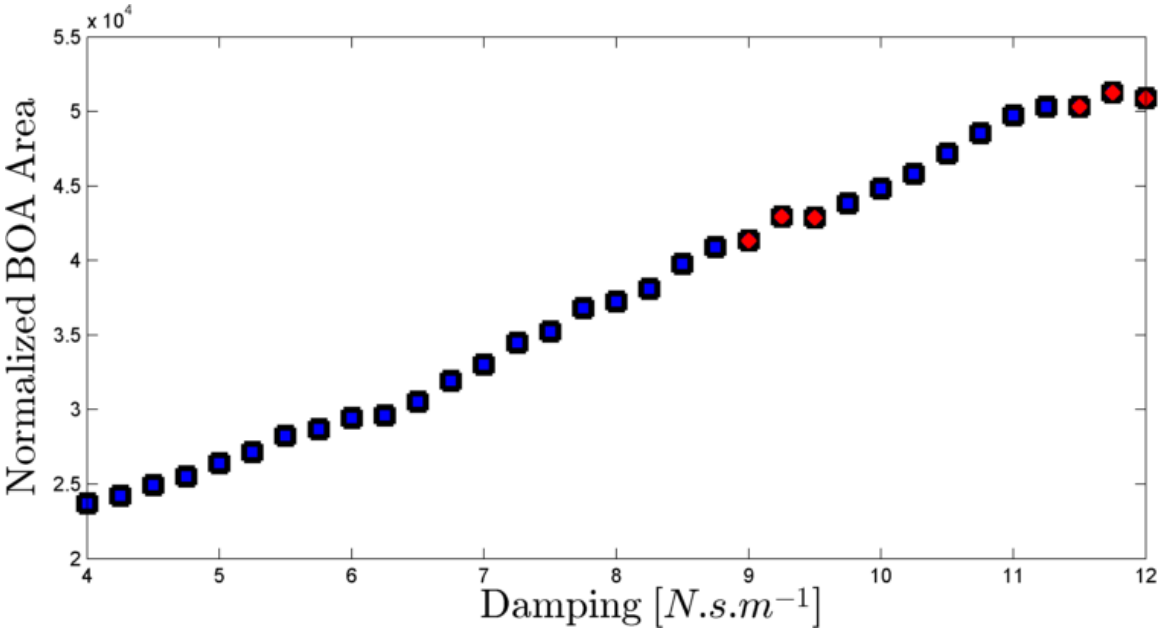

Figure A-8. The normalized basin of attraction plotted against damping values. The area of the basin of attraction was normalized to the search area of $1x10^{-12}$ $rad^2.s^{-1}$. The spring-damper values that were used to calculate the BOA were the most stable period-1 limit cycles in terms of Floquet multipliers. The stiffness values are between 26.0 $N.m^{-1}$ and 39.1 $N.m^{-1}$, and monotonically increasing as the damping values increase between 4 $N.s.m^{-1}$ and 12 $N.s.m^{-1}$. The areas in red are highlighted because the normalized BOA area is not monotonically increasing due to the presence of a separate attractor near the fixed point for which the BOA was calculated.

The BOA of an OPDW with a relatively large amount of damping is 135.1% larger than the BOA of the CPDW. The normalized BOA area is plotted in (Figure A-8). This plot illustrates that the area of the BOA monotonically increases or decreases as the bifurcation parameters are systematically increased. The areas of the BOA for the fixed points located in the left half of the dark blue arch (stiffness values between 26.0 $N.m^{-1}$ and 39.1 $N.m^{-1}$) in Figure A-4**Error! Reference source not found.** were calculated. A separate attracting limit cycle is nearby the attracting limit cycle of the calculated BOA at damping values of 9.5 $N.s.m^{-1}$ and 12.0 $N.s.m^{-1}$. However, the attracting limit cycle is closer to the border of the BOA and does not have a substantial effect. These attracting limit cycles could be analyzed further and their behavior may be substantially different.

Summary

The OPDWs presented dynamics that were both more complex and more stable than the CPDW. The attractors for the different limit cycles grew in complexity as the limit cycle bifurcated and eventually became chaotic. However, these analyses do not completely encompass the dynamics of the OPDW or CPDW. There are clearly attractors that are stronger and possibly more stable than the ones that were analyzed. Bipedal walking is highly nonlinear by design. Adding a soft tissue component illustrates that a larger spectrum of stability can be achieved by simply changing the spring-damper parameters of the OPDW. Furthermore, the soft tissue may be realized in a passive-dynamic walker with the addition of mass that oscillates. It has been illustrated through computer simulation that mass oscillation increases a PDWs robustness to terrain

roughness. It may be beneficial to add a soft tissue mass in order to increase a physical PDW's long-term stability.

Appendix B

Floquet Multiplier, Local Divergence Exponents, and Slope Perturbation Range Tables

Table B-1. A table of the spring-damper parameters that resulted in the most stable period-1 gait cycles in terms of Floquet multipliers for each damping condition. The range of slopes for which the OPDW and CPDW could ambulate and the normalized area of the basin of attraction was calculated for each spring-damper condition.

	c ($N.s.m^{-1}$)	k ($N.m^{-1}$)	Floquet Multiplier	Slope Range	BOA Area (Normalized)
Control	0	0	0.5883	0.0144	21798
Oscillating	0.00	0.7	0.4167	0.0144	28514
	0.25	0.7	0.4177	0.0142	29603
	0.50	0.7	0.4202	0.0138	30360
	0.75	0.7	0.4238	0.0136	30615
	1.00	0.7	0.4283	0.0132	30950
	1.25	0.8	0.4214	0.0130	29604
	1.50	0.8	0.4285	0.0129	30550
	1.75	0.9	0.4277	0.0127	30430
	2.00	0.9	0.4362	0.0127	30898
	2.25	1.0	0.4390	0.0128	31042
	2.50	1.1	0.4440	0.0128	29905
	2.75	1.3	0.4490	0.0140	29868
	3.00	1.4	0.4580	0.0140	30100
	3.25	1.4	0.4674	0.0141	30474
	3.50	25.8	0.3545	0.0155	22400
	3.75	25.9	0.3576	0.0161	23131
	4.00	26.0	0.3583	0.0160	23716
	4.25	26.1	0.3589	0.0164	24226
	4.50	26.2	0.3607	0.0162	24929
	4.75	26.3	0.3647	0.0211	25516
	5.00	26.5	0.3584	0.0210	26384
	5.25	26.6	0.3645	0.0209	27133
	5.50	26.8	0.3619	0.0208	28233
	5.75	27.0	0.3596	0.0207	28679
	6.00	27.1	0.3610	0.0208	29430
	6.25	27.3	0.3672	0.0207	29619
	6.50	27.5	0.3680	0.0205	30515
	6.75	27.8	0.3626	0.0204	31920
	7.00	28.0	0.3654	0.0205	33014
	7.25	28.2	0.3692	0.0204	34469
	7.50	28.5	0.3669	0.0203	35228
	7.75	28.8	0.3669	0.0203	36806
	8.00	29.1	0.3667	0.0202	37251
	8.25	29.4	0.3671	0.0201	38108
	8.50	29.8	0.3638	0.0200	39762
	8.75	30.1	0.3665	0.0201	40897
	9.00	30.5	0.3655	0.0176	41339
	9.25	30.9	0.3650	0.0176	42958
	9.50	31.3	0.3661	0.0177	42879
	9.75	31.8	0.3646	0.0178	43822
	10.00	32.3	0.3644	0.0176	44804
	10.25	32.8	0.3653	0.0181	45823
	10.50	33.4	0.3646	0.0181	47167
	10.75	34.0	0.3653	0.0183	48552
	11.00	34.8	0.3635	0.0184	49740
	11.25	35.6	0.3631	0.0182	50314
	11.50	36.4	0.3646	0.0182	50312
	11.75	37.6	0.3637	0.0189	51255
	12.00	39.1	0.3651	0.0189	50873

Table B-2. A table of the spring-damper parameters that resulted in the most stable period-1 gait cycles in terms of local divergence exponents for each damping condition. The range of slopes for which the OPDW and CPDW could ambulate was calculated for each spring-damper condition.

	c ($N.s.m^{-1}$)	k ($N.m^{-1}$)	Local Divergence Exponent	Slope Range
Control	0	0	1.0069	0.0144
Oscillating	0.00	6.0	1.0037	0.0057
	0.25	5.8	1.0025	0.0058
	0.50	5.6	1.0012	0.0078
	0.75	5.4	1.0000	0.0080
	1.00	5.2	0.9988	0.0082
	1.25	5.0	0.9976	0.0084
	1.50	4.8	0.9964	0.0094
	1.75	4.6	0.9952	0.0096
	2.00	4.6	0.9940	0.0100
	2.25	4.6	0.9927	0.0103
	2.50	4.6	0.9915	0.0106
	2.75	4.6	0.9904	0.0105
	3.00	4.6	0.9891	0.0105
	3.25	4.7	0.9879	0.0106
	3.50	55.5	0.9845	0.0194
	3.75	55.6	0.9834	0.0188
	4.00	55.7	0.9822	0.0185
	4.25	58.6	0.9810	0.0193
	4.50	58.2	0.9798	0.0191
	4.75	57.7	0.9787	0.0189
	5.00	57.2	0.9775	0.0186
	5.25	56.7	0.9763	0.0185
	5.50	56.4	0.9751	0.0183
	5.75	56.6	0.9740	0.0184
	6.00	56.8	0.9728	0.0185
	6.25	57.0	0.9716	0.0184
	6.50	57.2	0.9705	0.0184
	6.75	57.3	0.9693	0.0184
	7.00	57.4	0.9681	0.0184
	7.25	57.9	0.9669	0.0185
	7.50	57.9	0.9657	0.0184
	7.75	58.5	0.9646	0.0185
	8.00	61.9	0.9634	0.0192
	8.25	61.3	0.9622	0.0189
	8.50	60.6	0.9610	0.0188
	8.75	59.7	0.9598	0.0186
	9.00	168.2	0.9585	0.0184
	9.25	168.3	0.9574	0.0182
	9.50	168.3	0.9562	0.0181
	9.75	168.4	0.9550	0.0181
	10.00	168.4	0.9538	0.0179
	10.25	168.4	0.9526	0.0178
	10.50	168.4	0.9515	0.0177
	10.75	168.5	0.9503	0.0176
	11.00	168.5	0.9491	0.0176
	11.25	168.4	0.9479	0.0175
	11.50	168.4	0.9467	0.0174
	11.75	168.5	0.9456	0.0173
	12.00	168.3	0.9444	0.0171

Table B-3. A table of the spring-damper parameters that resulted in the most stable period-1 gait cycles in terms of the slope perturbation range for each damping condition. The resultant minimum and maximum slopes of the applied perturbation that were used to calculate the slope perturbation range are reported in the last two columns.

	c ($N.s.m^{-1}$)	k ($N.m^{-1}$)	Slope Perturbation Range	Min Slope	Max Slope
Control	0	0	0.0072	0.00525	0.01245
Oscillating	0.00	1.1	0.0093	0.00560	0.01490
	0.25	1.1	0.0093	0.00560	0.01490
	0.50	1.2	0.0094	0.00555	0.01495
	0.75	1.3	0.0097	0.00555	0.01525
	1.00	1.4	0.0098	0.00560	0.01540
	1.25	1.4	0.0098	0.00555	0.01530
	1.50	1.6	0.0100	0.00555	0.01555
	1.75	1.8	0.0101	0.00555	0.01560
	2.00	1.9	0.0102	0.00545	0.01560
	2.25	1.9	0.0100	0.00550	0.01545
	2.50	2.1	0.0101	0.00545	0.01550
	2.75	2.2	0.0100	0.00550	0.01545
	3.00	2.4	0.0099	0.00555	0.01540
	3.25	2.6	0.0098	0.00555	0.01535
	3.50	53.7	0.0167	0.00340	0.02010
	3.75	53.5	0.0164	0.00345	0.01980
	4.00	53.3	0.0161	0.00345	0.01955
	4.25	53.1	0.0159	0.00350	0.01935
	4.50	52.9	0.0156	0.00355	0.01910
	4.75	52.6	0.0153	0.00365	0.01890
	5.00	52.6	0.0151	0.00360	0.01865
	5.25	52.1	0.0148	0.00370	0.01850
	5.50	52.0	0.0147	0.00365	0.01830
	5.75	51.6	0.0144	0.00370	0.01810
	6.00	51.2	0.0142	0.00380	0.01800
	6.25	50.8	0.0141	0.00375	0.01785
	6.50	50.5	0.0139	0.00385	0.01770
	6.75	50.5	0.0137	0.00380	0.01750
	7.00	49.6	0.0136	0.00385	0.01745
	7.25	49.3	0.0134	0.00385	0.01725
	7.50	48.6	0.0133	0.00390	0.01715
	7.75	48.1	0.0131	0.00395	0.01700
	8.00	47.4	0.0130	0.00395	0.01695
	8.25	46.7	0.0129	0.00395	0.01680
	8.50	45.7	0.0126	0.00400	0.01660
	8.75	44.4	0.0124	0.00400	0.01640
	9.00	156.5	0.0144	0.00385	0.01825
	9.25	155.8	0.0142	0.00390	0.01805
	9.50	155.2	0.0139	0.00395	0.01780
	9.75	154.5	0.0135	0.00405	0.01755
	10.00	153.4	0.0134	0.00405	0.01740
	10.25	156.0	0.0130	0.00405	0.01705
	10.50	151.6	0.0128	0.00415	0.01695
	10.75	315.4	0.0137	0.00405	0.01770
	11.00	317.7	0.0134	0.00405	0.01745
	11.25	321.1	0.0132	0.00405	0.01725
	11.50	320.4	0.0130	0.00410	0.01705
	11.75	319.4	0.0128	0.00415	0.01690